IEEE Access
Multidisciplinary ⋮ Rapid Review ⋮ Open Access Journal

Received September 3, 2020, accepted September 27, 2020, date of publication October 1, 2020, date of current version October 14, 2020.

Digital Object Identifier 10.1109/ACCESS.2020.3028224

A Novel FBG-Based Triggering System for Cardiac MR Imaging at 3 Tesla: A Pilot Pre-Clinical Study

JAN NEDOMA[1], RADEK MARTINEK[2], (Member, IEEE), MARCEL FAJKUS[1], JINDRICH BRABLIK[2], RADANA KAHANKOVA[2], MICHAEL FRIDRICH[1], MICHAL KOSTELANSKY[1], PAVLA HANZLIKOVA[3], LUBOMIR VOJTISEK[4], AND KHOSROW BEHBEHANI[5], (Fellow, IEEE)

[1]Department of Telecommunications, Faculty of Electrical Engineering and Computer Science, VŠB–Technical University of Ostrava, 708 00 Ostrava, Czech Republic
[2]Department of Cybernetics and Biomedical Engineering, Faculty of Electrical Engineering and Computer Science, VŠB–Technical University of Ostrava, 708 00 Ostrava, Czech Republic
[3]Department of Imaging Method, Faculty of Medicine, University of Ostrava, 703 00 Ostrava, Czech Republic
[4]Central European Institute of Technology (CEITEC), Masaryk University, 601 77 Brno, Czech Republic
[5]Department of Bioengineering, The University of Texas at Arlington, Arlington, TX 76019, USA

Corresponding author: Jan Nedoma (jan.nedoma@vsb.cz)

This work was supported in part by the Ministry of Education of the Czech Republic under Project SP2020/156 and Project SP2020/38, in part by the European Regional Development Fund in the Research Centre of Advanced Mechatronic Systems Project within the Operational Programme Research, Development and Education under Project CZ.02.1.01/0.0/0.0/16_019/0000867, in part by the Grant Programme Support for Science and Research in the Moravia-Silesia Region 2018 under Grant RRC/10/2018, and in part by the MEYS CR (Czech-BioImaging) for the Core Facility Multimodal and Functional Imaging Laboratory (MAFIL) of Central European Institute of Technology (CEITEC) under Grant LM2018129.

ABSTRACT This first-ever study demonstrates the applicability of a fiber Bragg grating (FBG) system for MR cardiac triggering of cardiovascular magnetic resonance at 3 Tesla. The unique patented system senses body movements caused by cardiac activity using a non-invasive ballistocardiography (BCG) sensor. The pilot research compares a novel FBG-based system with clinically used triggering systems based on electrocardiography (ECG) and pulse oximetry (POX). The pilot pre-clinical study was conducted on 8 subjects at a Siemens Prisma 3T MR Scanner. The study compares images from two basic cardiac sequences, TRUE FISP (Free Induction Decay Steady-State Precession) and PSIR (Phase Sensitive Inversion Recovery), using objective methods and subjective evaluation by clinical experts. The study presents original results that confirm the applicability of optical sensors in the field of cardiac triggering having a number of advantages in comparison to conventional solutions, such as no eddy current interference, ease of placement of the sensor on the patient's body, and senor reusability. The proposed FBG-based system achieves comparable results with the most frequently used and most accurate ECG-based and POX-based clinical systems. In terms of subjective evaluation by experts, the FBG system outperformed the POX-based system used in clinical practice.

INDEX TERMS Fiber Bragg grating (FBG), optic system, cardiac triggering, electrocardiography (ECG), pulse oximetry (POX), magnetic resonance imaging (MRI).

I. INTRODUCTION

Magnetic Resonance Imaging (MRI) is a widely applied clinical diagnostic and prognostic imaging system with high sensitivity and superior specificity. Building on more than 30 years of MRI clinical applications, the research on improvement of this imaging modality is continuing. Of particular importance is the research efforts aimed at improving the quality of acquired images despite the image distortion naturally induced by respiration [1], [2] and cardiac function [3]–[5], as movement of patient body degrades the quality of acquired images [6]–[8]. Since the movements due to respirator and cardiac function are unavoidable [9], researchers have explored ways of compensating for such movements. Specifically, such compensations are based on detecting the time points when the body displacement is minimal and triggering the acquisition of the MRI images at that instance, for brevity, referred to as triggering.

Currently, there are two types of triggering: prospective triggering [10] and retrospective gating [11]. Prospective

The associate editor coordinating the review of this manuscript and approving it for publication was Ilaria Boscolo Galazzo.

triggering is based on detecting a specific point in either the cardiac or respiratory cycles and triggering the MRI acquisition according to a selectable delay. Typically, the delay is selected in such a way that the scan of the organ under examination could be captured at the time of minimal movement. For example, when imaging the heart, the end of the diastole is chosen to coincide with maximal expansion of the ventricles [12]. Retrospective triggering is based on first recording and analyzing the cardiac or respiratory function. Then, the triggering of the acquisition of the MRI images is made based on previously recorded and analyzed cardiac or respiratory data, without a link to the current value of such signal. Prospective triggering is generally preferred as it allows a given system to respond to present changes in cardiac or respiratory data [13] and [14]. The accuracy of the examination is significantly influenced by the stationarity of the area being examined. Motion of the examined area can cause distortion of the image. Most often, these motion artefacts cause ghost images or diffuse image noise in the phase-encoding direction [6]–[8]. It is practically impossible to make the area completely immobile, both as for the physiological functions of the organs being captured (especially the heart and the lungs) [9] and as for the limited cooperation of the subject itself (body movements, insufficient breath retention). A brief description of the current MRI triggering approaches is provided in following section II.

This is a first study describing the use of purely fiber optic technology for cardiac triggering for MRI scans, which is now based on ECG and POX measurements that face several limitations (see section II-A for more information). As reported in our earlier work, we have demonstrated the capabilities of FBG-based optical sensors for vital sign monitoring [15]–[17]. These investigations provided the foundation for the sensor evaluation in the MR environment that is present in the current paper [15]–[21]. As will be detailed in this article, the proposed FBG-based sensor offers multiple advantages that includes continuous monitoring of the patient vital signs, simultaneous monitoring of respiratory and cardiac activities, and not being affected by the magnetic field of the MRI. Further, the proposed system does not require complicated manufacturing processes. This allows the system to be highly accurate and feasible for clinical practice.

The results accomplished using the innovative FBG sensor are evaluated in terms of quality of the resulting MR images during cardiac triggering and compared to conventional signal measurement approaches using ECG and POX. The applicability of the proposed FBG-based system was analyzed using objective parameters of image quality evaluation as well as using subjective evaluation of images by clinical experts (radiological assistants and physicians).

II. STATE-OF-THE-ART TRIGGERING METHODS

There are currently two types of triggering – prospective triggering [10] and retrospective gating [11]. In the case of prospective triggering, scanning is activated by a change in the vital sign, which means we are waiting for the organ activity that is detected and, accordingly, MR acquisition is triggered with a defined delay. The delay is defined in such a way that the organ under examination could be captured at the time of minimal movement, for example, the heart at the end of the diastole, when the ventricles of the heart are maximally expanded. In retrospective gating, physiological functions are first recorded and analyzed and, on this basis, an acquisition is made, but now without a link to the current value of the biological signal. Prospective triggering is generally preferred as it allows a given system to respond to irregularities in vital signs, see [13], [14].

The principle of triggering is to detect the most prominent point of the signal that indicates the cardiac systole. In current clinical practice, cardiac activity sensing using these two methods prevails:

a) *Electrocardiography* is based on recording electrical potentials between three electrodes placed on the chest surface. The biological signal obtained, the electrocardiogram (ECG), contains several important features, the most significant of which is the so-called R wave, corresponding to the depolarization of the ventricles. Accurate triggering based on ECG is conditioned by obtaining a prominent R wave, whose morphology is significantly influenced by the positioning of the measuring electrodes [22], [23].

b) *Photoplethysmography* is based on monitoring the peripheral pulse of the blood, which is performed using a unit attached to the finger of the person examined. The measurement is conducted using a POX sensor placed on the subject's finger; the POX sensor consists of two main components - a LED (Light-Emitting Diode) and a photodiode or a phototransistor. The LED is a light source here, while the photodiode or the phototransistor is its detector. As the volume of blood in the illuminated portion of the tissue changes, the intensity of the light detected varies linearly. The heart rate can then be determined from this pulsing signal. This type of monitoring is more suitable for the above-mentioned retrospective gating [24], [25].

Alternative methods used for CMRI include:

a) *Seismocardiography (SCG)* monitors the mechanical manifestations of the heart, which present as chest movements (vibrations). These vibrations are sensed using a suitably positioned sensor [26]–[28].

b) *Phonocardiography (PCG)* focuses on sensing acoustic manifestations of the heart, the so-called heart sounds. These manifestations are recorded by means of a chest sensor and converted to electrical voltage by microphones located close to the patient's body surface or at the end of the acoustical system [29], [30].

c) *Ballistocardiography (BCG)* is based on sensing blood movement in large blood vessels. The BCG signal is measured using various sensors capable of sensing pressure, such as optical [31], [32] or mechanical ones [33], [34].

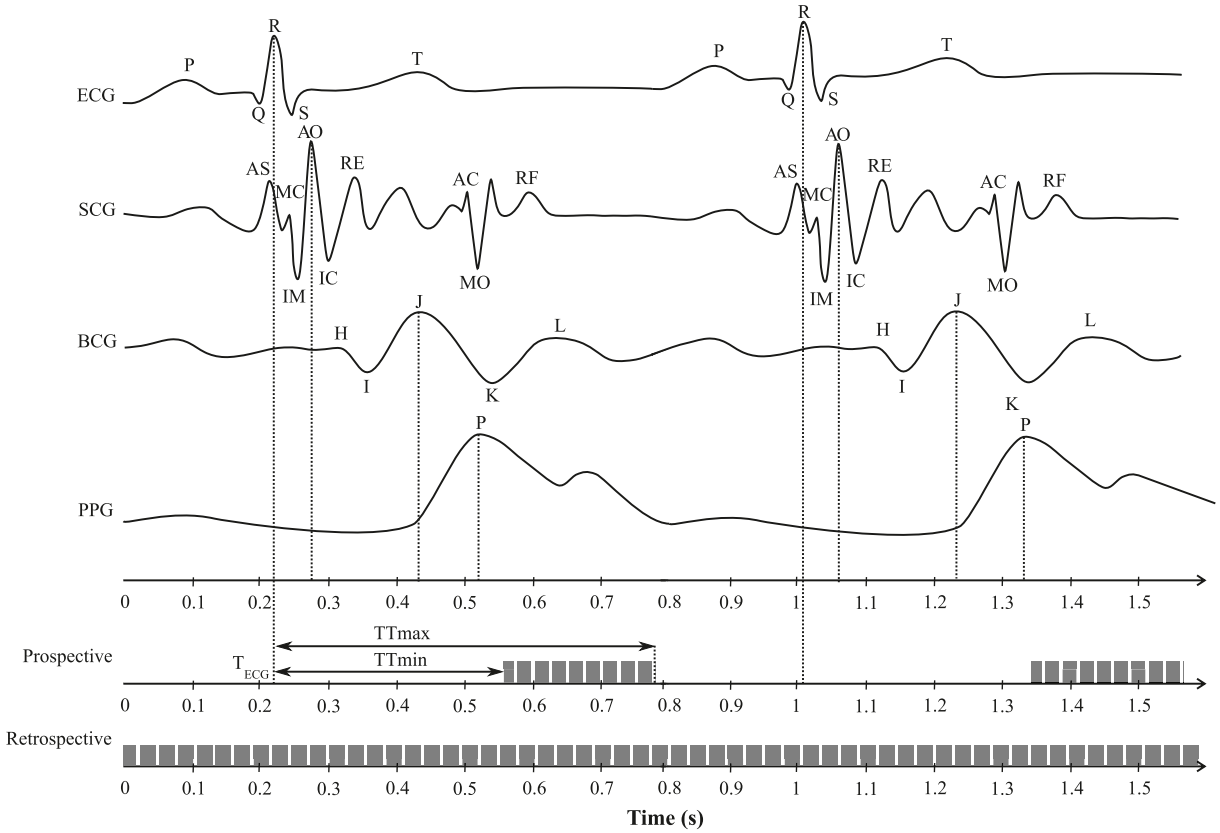

FIGURE 1. Physiological delay between MR triggering signals with marked triggering pulses for clinically used methods, including signals within alternative methods.

When triggering the MR scanner using different signals, it is important to keep in mind their physiological delay. This results in the fact that the corresponding significant points are not detected at the same time T. The cardiac activity is initiated by electrical activity generated in the cardiac conduction system, so it is clear that mechano-acoustic heart signals sensed will always be delayed compared to the ECG signal, i.e., $T_{ECG} < T_{SCG}, T_{BCG}, T_{PPG}, T_{PCG}$.

Fig. 1 illustrates the principle of two types of triggering using an ECG signal. Retrospective gating performs continuous heart sensing regardless of the current state of the corresponding biological signals. The resulting image is then reconstructed from the sub-images using a simultaneously measured ECG signal, so that the image was as little blurry and noisy as possible. On the other hand, the prospective gating (triggering) method is based on taking a single image at such a phase of the heart cycle, where the heart is relatively still. An example of such still phase in the ECG signal is the time interval between the end of the T wave and the beginning of the P wave in the forthcoming heart cycle. The MR scanner is triggered with a time delay after the R wave detected in the ECG signal at time T_{ECG}. This delay α is defined by the physiological duration of each significant point and its extreme values define the maximum and minimum time points (TT_{min}, TT_{max}) in which it is possible to perform a successful MR triggering. For prospective triggering (TT_P) using an ECG signal, triggering time can, therefore, be defined as follows:

$$TT_P = T_{ECG} + \alpha, \tag{1}$$

where $\alpha \in (TT_{min}, TT_{max})$. This value varies with different biological signals.

The principle of heart rate measurement using an optical Fiber Bragg Grating (FBG) sensor is based on BCG and has been described previously [35]–[47]. Cardiac activity is manifested physiologically in the chest area by a slight pressure action occurring due to the mechanical activity of the heart. This phenomenon causes pressure on the sensor located in the chest (heart) area of the human body. A suitably positioned and encapsulated sensor can detect these weak heart signals.

A. LIMITATIONS OF CONVENTIONAL METHODS

Classical methods used in clinical practice have their disadvantages and limitations of use. For ECG-based triggering, it is necessary for the curve obtained to have a prominent R wave, wherein achieving a prominent R wave is conditioned by the placement of the electrodes. Superposition of interferences caused by the MR scanner gradients and the magnetohydrodynamic effect can cause a spurious effect in R wave detection [48]. This effect is based on the formation of small induced potentials in a strong magnetic field, which causes changes in the potential of cell membranes [49]. The

effect described above leads to ECG signal distortion by affecting the T wave morphology (see Fig. 2), thus preventing proper detection of the R wave and the subsequent synchronization [50].

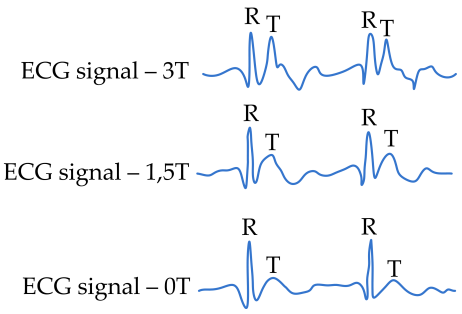

FIGURE 2. Effect of magnetic field on the ECG morphology.

The problems associated with this effect grows with the increasing intensity of the magnetic field [51]. Recording of vital signs using electrodes and three-lead ECG may be limiting with many patients. It is often a problem to find the right position of the electrodes; this effect is also evident in relation to gender, where placement on women is complicated. Another condition is good adhesion of the electrodes; with men, it is appropriate to shave and clean the required area.

A frequent problem of triggering with the ECG curve is the necessity of patient cooperation. It is necessary to modulate the inhalation depth, since, in the case of a significant inhalation, the R wave detection is difficult or impossible, which extends the time of the sequence being collected and possibly prevents the sequence from completing [10], [13].

These triggering methods have many drawbacks. As a result, new techniques and sensors for cardiac sensing for the purpose of triggering a cardiac magnetic resonance imaging (CMRI) acquisition are continually being developed. Some of the methods being developed have already been used in clinical practice, one of which is the so-called self-gating technique, see [52] and [53]. In this method, information about organ movements obtained from the MR signals is processed by monitoring the changes in the total transverse magnetization. Moreover, this technique does not require number of sensors placed on the patient's body, which can be considered as one of its benefits. On the other hand, it should be noted that these techniques lag behind at very high MR field gradients in cases where myocardial contraction and relaxation are very weak throughout the entire heart cycle [54] and [55].

B. RESEARCH FOCUSED ON THE USE OF ALTERNATIVE TRIGGERING METHODS

1) PHONOCARDIOGRAPHY (PCG) AND SEISMOCARDIOGRAPHY (SCG)

Examples of practical use of acoustic methods are studies [56]–[58], and [59], which presented the use of an acoustic sensor in an MR environment. The solutions proposed were tested on devices with different magnetic field strengths. The use of acoustic sensors offers several major advantages. The main advantage is the resistance of the acoustic signal to the magnetic field of the MR device. Compared to conventional methods, it also has the advantage of reducing the number of cables and sensors, thereby simplifying and speeding up patient preparation [55], [56]. Several ways to perform sensing using an acoustic sensor are described. Frauenrath *et al.* [60] described the use of an acoustic waveguide for transmitting a signal to an MR unit, where the signal is filtered because of acoustic noise generated by switching of gradient coils. Another possibility is to convert the acoustic signal to an optical one, where the waveguide is replaced by optical fiber, so the negative influence on the sensing device is completely eliminated (Maderwald *et al.* [56]). According to earlier research (Becker *et al.* [55]), the delay (approximately 30 ms) between the first heart sound and the R wave in ECG signal has no effect on CMR imaging by means of retrospective triggering. Other research [57], for change, shows that triggering by an acoustic signal, even in a magnetic field with an intensity of up to 7 T, can achieve an error of less than 1%.

Seismocardiography is another option for measuring cardiac activity in the MR environment and the subsequent triggering of the MR scanner [26]–[28]. The authors of the study have already developed a hybrid acoustic sensor for MR triggering based on SCG [26], the foundation of which is sensing vibrations of the human body surface due to the movement of the heart wall commonly sensed by accelerometers. Although this sensor achieved very satisfactory results in some subjects measured, the system faced problems associated with placing the sensor itself on the patient's body, resulting in a deterioration in the quality of detection of significant points (A0-A0), thus in worse CMRI synchronization.

2) FIBER-OPTIC SENSORS

The most modern methods for measuring medical signals nowadays include optical fibers and fiber-optic sensors that are immune to electromagnetic interference when properly designed [35]–[47]. These sensors offer a relatively inexpensive and technically undemanding alternative to CMRI triggering.

There are not many studies on the use of fiber-optic technology for monitoring the vital signs of the human body in MR environments. One of the most interesting studies presents Dziuda *et al.* [31], which described an FBG-based sensor encapsulated on the plexiglass board. The results were obtained from three patients during the MRI scanning and proved the method is able to determine both the respiratory and heart rate accurately.

Moreover, there is a study [61] that describes a sensor which is embedded as a smart textile solution that can be used within the patient's clothes. The detection of the respiratory and heart rates was accurate even when the user was performing periodic body movements, such as the ones induced by the gait. The authors declare that the proposed approach

can be applied not only in MRI environments and in patient monitoring during the sleep, but also as an e-health solution for continuous monitoring of the patients during their daily activities.

Interesting FBG-embedded smart textiles were proposed for respiratory monitoring during MR examinations in [62]. The comparison of the results obtained by the system and by optoelectronic plethysmography highlights the accuracy in the estimation of the respiratory period, duration of the inspiratory and expiratory phases. Summarization of the use of fiber-optic sensors for monitoring the basic vital signs of the human body is well described in [29], where a total of 47 MR-tested or potentially MR-compatible sensors have been described, but no study described the practical implementation of cardiac triggering in real MR environments.

As for the cardiac triggering method using fiber-optic sensors, only a few studies, which investigate the possibility of cardiac triggering, but only when used in rodents, are described [63]. The sensor was orally introduced into the rat's oesophagus [64] or was placed on the thorax [65] the movement of which it senses.

In our previous research [17], we discussed the novel sensor which is created by encapsulation of the Bragg grating into conventional nasal oxygen cannulas. Respiratory triggering functionality was confirmed by radiologists on the basis of analyzing images by means of the most commonly used respiratory triggered T2 TSE 3D sequences and by means of an objective method using the Blind/Referenceless Image Spatial Quality Evaluator (BRISQUE).

III. MATERIAL AND METHODS

Based on the background research and the current state of the technology for cardiac triggering, we have developed an innovative FBG sensor utilizing a combination of polymeric material, polydimethylsiloxane (PDMS), and FBG [66]. PDMS has desirable properties, such as immunity to electromagnetic interference, inertness to human skin, minimal effect on the FBG function, and protection of the FBG part of the sensor. The sensor used in this study has evolved from our team's previous biomedical applications experience [15], [18]–[20]. The sensor was fabricated using a 3D printing process.

A. FIBER BRAGG GRATING (FBG)

Bragg gratings are usually used as the sensing elements in optical fiber sensors used to measure various physical quantities such as pressure and temperature [67]. They are constructed by inscribing periodic variation in the refractive index of the core of an optical fiber, as shown in Fig. 3, where the periodic refractive index of the core is denoted by n_1 and the non-periodic refractive index of the sheath is labelled as n_2. When a high intensity light source (e.g., Light-Emitting Diode - LED) with a relatively broad spectrum is input to the FBG sensor, the reflected light will have a relatively narrow spectrum with a peak at a wavelength that is function of the optical and geometric properties of the FBG. Specifically, the spectral position of the Bragg wavelength, λ_B, is affected

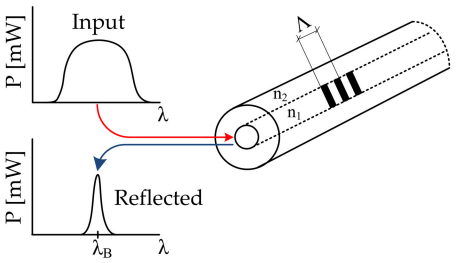

FIGURE 3. The principle of operation of a Bragg grating in the optical fiber core.

by the optical and geometric properties of the periodic structure according to (2):

$$\lambda_B = 2n_{eff}\,\Lambda, \tag{2}$$

where n_{eff} is the effective refractive index of the periodic structure and Λ is the period of the refractive index change in the optical fiber core.

This property of FBG is used in sensor design where the temperature or pressure causes a change in the optical and geometric properties of the structure and a shift in the Bragg wavelength according to (3):

$$\frac{\Delta\lambda_B}{\lambda_B} = (1 - p_e)\varepsilon + (\alpha_\Lambda + \alpha_n)\Delta T, \tag{3}$$

where p_e is the photo-elastic coefficient, ε is the applied deformation, α_Λ is the coefficient of thermal expansion, α_n is the thermo-optic coefficient and ΔT is the temperature change. Typically, when the temperature sensitivity of the fiber optic Bragg grating reaches 10.3 pm/°C at 1,550 nm and the strain sensitivity achieves 1.209 pm/μstrain [68].

B. FBG SENSOR DESIGN

To construct our FBG sensor we used an optical fiber ITUT recommendation G.652 which describes the geometrical, mechanical, and transmission attributes of a used single-mode optical fiber and cable [69] with uniform Bragg grating and acrylate recounting (Safibra, Prague, Czech Republic) and the Bragg grating with central Bragg wavelength of 1550.121 nm and reflectivity of 95.8 %. To protect the optical fiber and to increase its sensitivity while monitoring human cardiac activity, we used the PDMS Sylgard 184 polymer [70]. The curing of the polymer took place at an elevated temperature of 80 C for 90 minutes. Sylgard 184 was chosen as a product that exhibits excellent heat resistance and elastic properties. More importantly, it is harmless to human and is electrically nonconductive. We have previously reported successful encapsulating of the Bragg grating sensor and its use in several biomedical application [15], [18]–[20].

Based on recent refinements, we now have achieved minimum dimensions of 30 × 15 mm and weight of 2 g resulting in simpler implementation and minimal load burden on the patient. Fig. 4 shows the proposed sensor prototype and illustrates its small dimensions suitable for clinical use. The encapsulation process has no significant effect on the

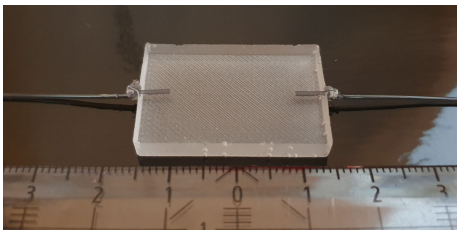

FIGURE 4. Novel fiber Bragg grating sensor.

functionality of the Bragg grating and its spectral characteristics; it only increases about 4.2 times the temperature sensitivity [71].

C. DESCRIPTION OF THE MEASURING HARDWARE AND SOFTWARE

Fig. 5 shows the schematic diagram of the measuring and triggering system. The FBG interrogator unit (FBGuard 1550 Fast, Safibra, Prague, Czech Republic) was placed in the MRI control room. This interrogator unit is designed for highly accurate static and dynamic measurements of FBG sensors monitored at up to 16 optical channels, the output power of superluminescent light emitting diode (SLED) is 1 mW. It is a fully autonomous system with an embedded computer and a web server running on Linux. The system configuration and configuration of sensors is possible by SSH and the web interface. An Ethernet interface allows remote connection to any standard computer (PC) through the TCP/IP protocol. A standard 8 m long fiber-optic cable (SMF, ITU-T, G.657.A) was used to connect the FBG interrogator unit to the FBG sensor.

The FBG interrogator unit is based on the spectral evaluation of Bragg wavelengths reflected from FBG sensors [72]. The unit consists of a broad-spectrum (1510-1590 nm) SLED, which emits the light which is then is guided through a circulator to FBG sensors. The reflected spectral contributions from the connected FBG sensors are fed through a circulator to a diffraction grating, which directs the light of individual wavelengths to a Charge-Coupled Device (CCD) detector with 512 px (i.e. 512 photodetectors in a row). This ensures the wavelength conversion at the pixel position in the CCD detector to obtain information on the spectral distribution of the received optical signal.

In terms of signal processing, peaks corresponding to individual FBG sensors are investigated. For analysis of the reflected spectrum, the interpolation method with the analytical Gaussian function is used to find the spectral position of individual Bragg wavelengths. This achieves a spectral resolution of 1 pm at 512 px on a CCD detector for the width of 1510 to 1590 nm.

The signal from the FBG sensor is acquired by the FBG interrogator unit is embedded in a computer and operates autonomously. It is capable of simultaneously sampling 16 optical channels. Since the FBG interrogator unit does not provide digital outputs it cannot be used to generate a triggering signal for MRI sequences. Hence, we incorporated a second personal computer (Acer Aspire 5 A515-51G-561D) with Windows 10 Home and a National Instrument compact data acquisition chassis (cDAQ - 9185, Austin, Texas, USA) to analyze the optical signal sensed by the FBG sensor and the FBG interrogator unit. The NI cDAQ-9185 chassis has four slots for I/O modules and Ethernet for communication interface. Further, the PC was programmed to generate the triggering signa. The data acquisition and triggering programs were created using the National Instruments LabView programming environment (National Instruments, Austin, Texas, USA) [73]. Data transmission between the FBG interrogator unit, the cDAQ chassis, and the PC for data analysis was accomplished using Ethernet. Further, we used a local network timing protocol server to synchronize the timestamps of the FBG interrogator unit computer and the PC. The cDAQ chassis has slots that allow to connect different I/O (Input/Output) modules. Additionally, to generate the triggering signal, we used an NI-9472 compact controller module with 8 digital output channels compatible in the range from 6V to 30 V with the capability of delivering currents up to 0.75 A per channel. Fig. 6. shows the details of the system hardware (upper part) and triggering algorithm (lower part) and a more in depth description of the system can be found in [17].

As shown in Fig. 6, the Triggering PC runs the LabVIEW application as the transfer control protocol (TCP) server. The signal from the FBG sensor is acquired by the FBG interrogator unit using a multichannel light-to-voltage (LTV) converters and single multiplexed analog-to-digital converter (ADC). The FBG unit is embedded in a computer and operates autonomously.

The data from the client are transmitted in packets of 10 samples, where each sample is acquired with a frequency of 1 kHz. Using the local network timing protocol server, each packet is given a timestamp for the first sample in each packet. This timestamp is used to calculate the time necessary for generating the triggering signal.

The first step of optical signal processing is bandpass filtering by a 2^{nd} order Butterworth approximation infinite impulse response (IIR) filter with a low cut-off frequency of 4 Hz and a high cut-off frequency of 20 Hz. This step is necessary for extracting the BCG component from the optical signal that mainly contains information about the subject's respiratory, on the basis of which the BCG signal is modulated [16]. IIR filter implementation was selected for its simple structure and low computational demands. Moreover, the choice of second order filter offers low signal delay and phase distortion. This step is necessary for extracting the BCG component from the optical signal that mainly contains information about the subject's respiratory activity, on the basis of which the BCG signal is modulated.

The proposed method is based on the so-called ballistocardiography. It is a medically certified method that senses body movements that are caused by cardiac activity. In particular,

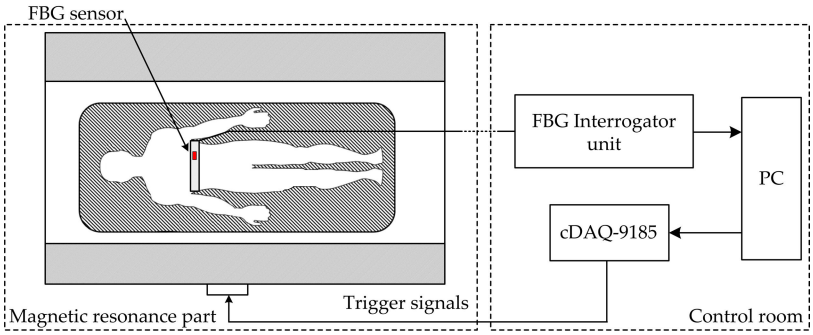

FIGURE 5. The schematic diagram of the FBG-based system applied to control the triggering of MRI scanner.

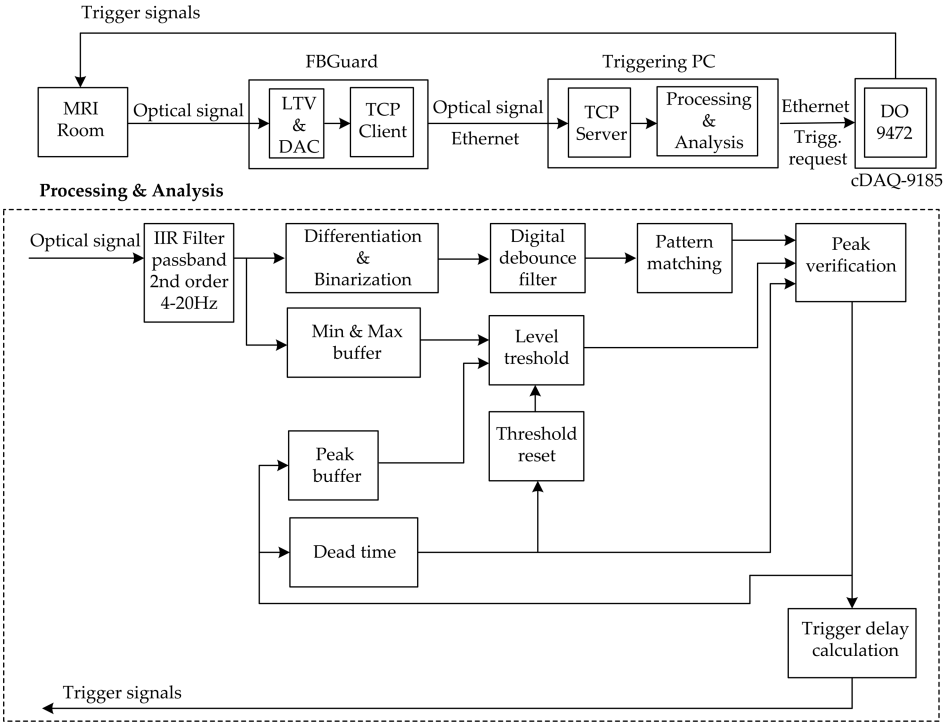

FIGURE 6. A block diagram of the measuring and triggering system with a detail of processing of the optical signal measured.

the output corresponds to the blood movement affecting the aortic arch, which causes the selected body parts to move upwards and downwards as the blood descends. This mechanical movement of the heart or chest affects the used FBG sensor placed on the patient's body and this is reflected in the shift of the Bragg wavelength.

Fig. 7 shows a sample of the signal measured by the FBG sensor and the extracted BCG component. The extracted BCG component is then analyzed by a peak detection algorithm based on the principle of signal derivation followed by its binarization. The binarized signal is then processed by pattern matching and a peak verification algorithm. Two conditions must be met to initiate this process: 1) the signal level exceeds a dynamically computed threshold, and 2) the time elapsed since the last trigger detected exceeds a dead time value that is configured by the user. The dead time mentioned for the condition 2 for triggering refers to the time interval during which one does not expect another peak to occur. Regarding the first condition, the dynamic peak threshold level value is determined by the peak detection algorithm and is based on an average value calculated from the buffer of the detected signal extremes (i.e., either minimum or maximum). A threshold levelling coefficient, ranging from 0 to 1, is used to scale the current peak threshold level value. The value of this levelling coefficient typically falls in a range of 0.5 to 0.8. When no peak is detected for more than 5 s, then the entire peak detection algorithm is reset (the extreme buffer is cleared).

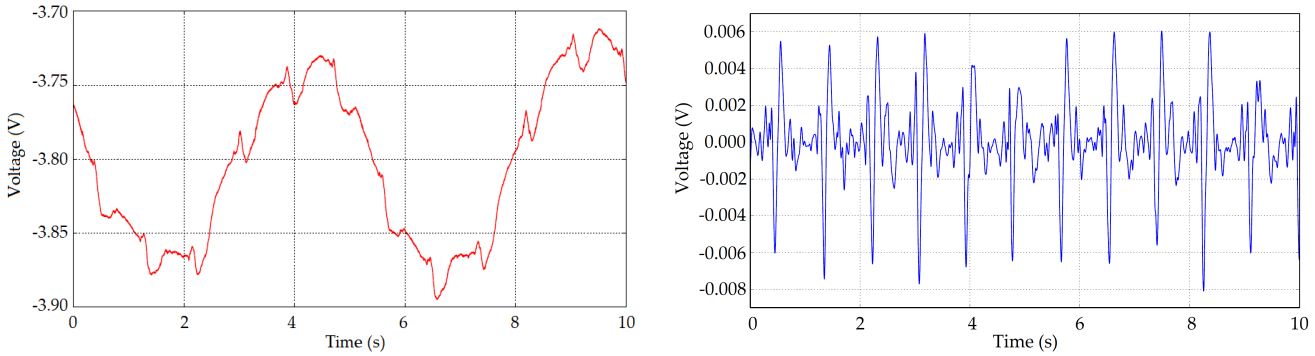

FIGURE 7. Examples of the signals measured and extracted. a) A time sample of the signal measured by the FBG sensor including components corresponding to the respiratory and cardiac activity; b) the BCG component extracted therefrom.

Positive or negative peaks can be utilized for triggering; these peaks correspond to I and J peaks of a typical BCG signal [74]. It is advantageous to select the negative peak since it precedes the positive one and thus offers a lower delay from the R peak of the ECG signal, which is used in conventional triggering systems. When a peak is successfully detected, the time to generate the triggering signal is calculated and a request to generate the signal is sent to the cDAQ chassis. The trigger signal time calculation includes the signal processing time, the delay caused by the IIR filter and the expected delay caused by communication between the triggering PC and the cDAQ chassis, which is very stable due to peer-to-peer connection. Fig. 8, shows an example of the BCG signal with the detected peaks along with the generated triggering signal.

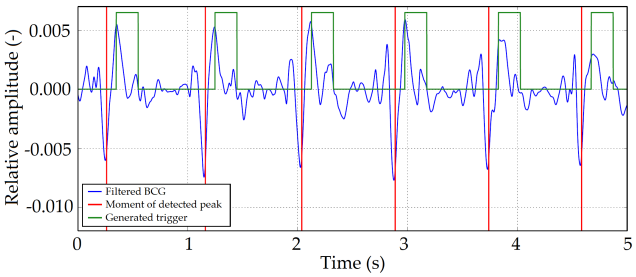

FIGURE 8. A time sample of the filtered BCG signal (blue) with the peaks corresponding to heartbeats detected (red) and the triggers generated (green).

D. OPTIMAL SENSOR PLACEMENT

The BCG signal corresponds to the movements of the human body surface caused by the acceleration of blood as it moves inside the large vessels. The blood also interacts with the individual parts of the heart, particularly the valves, which is reflected as the individual heart sounds as illustrated by Fig. 9. When placing the sensor to different locations, the morphology of individual BCG waveforms is affected by the size of contact area between the patient's body and the sensor, and the pressure applied on it. To find the optimal placement, we performed experiments on several volunteers in laboratory conditions (outside the MR environment). The aim was to find the location that would provide the BCG signal containing the significant peaks of high magnitude that could be easily detected and used to determine the heart rate.

Area for the sensor placement was selected based on a physician recommendation who used a stethoscope to examine each patient for heart auscultation. Points of auscultation over the precordium are generally correlated with the position of the cardiac valves [75] (see Fig. 9a and 9b). Besides the acoustic heart activity, the mechanical activity (body movement) can be sensed in the same areas due to the rise and fall of thorax due to heartbeats [75], see Fig. 9c.

The highest pressure is present in the mitral and tricuspid valve. The BCG signal reflects the pressure caused by the heart contraction, which reaches the peak in the ventriculi during the systole. Therefore, the BCG-based sensor should be placed as close to these areas as possible. That is, it should be placed between the sensing points denoted by (3) and (4). The optimal placement (marked in blue) was selected as a compromise between clinical feasibility for both male and female patients and the quality of the BCG signal (i.e., the magnitude and the shape of important features).

E. DESCRIPTION OF EXPERIMENTS

The experimental measurements were conducted in a 3 T magnetic resonance environment on a sample of 8 healthy people (4 male and 4 female). The patients signed a written consent that was approved by the Ethics Committee. The age range of the subjects was from 24 to 56 years, the weight ranged from 47 to 93 kg. The blood pressure was measured after a 15-minute rest period in the waiting room - sitting position, 15 minutes before preparation for measurement began. Additional demographic information of the subjects is summarized in Table 1; the range is defined by the mean along with the maximum and minimum values. The subjects were scanned by means of triggered sequences used for MR imaging of the heart. Because they were healthy volunteers, no contrast agent was administered.

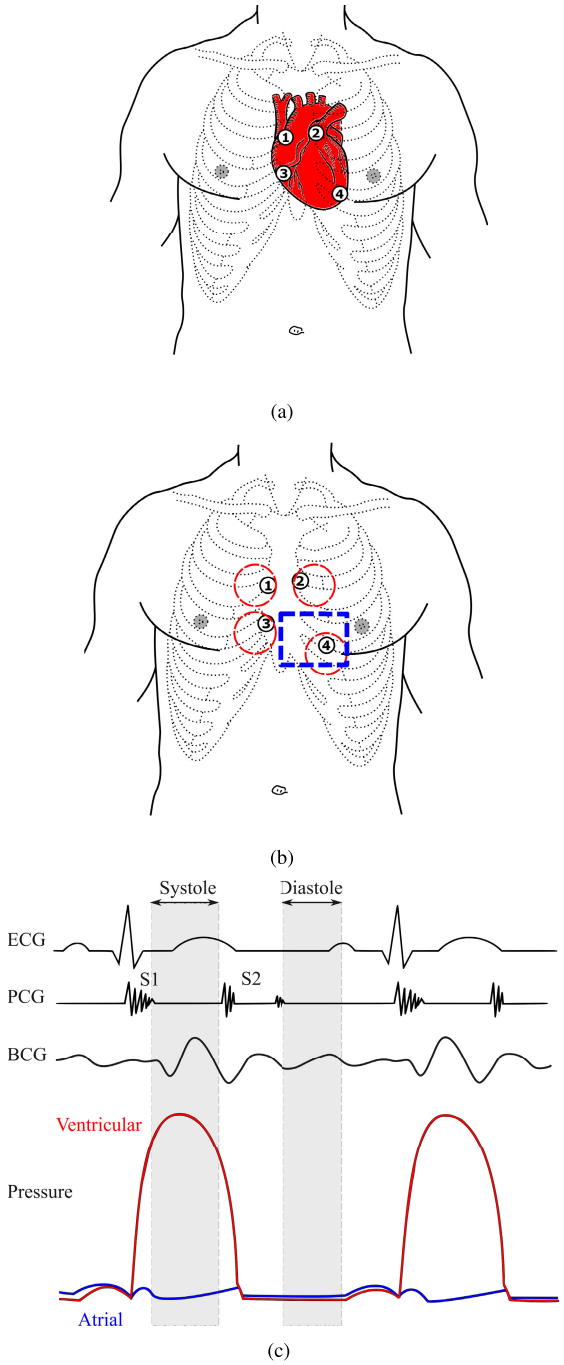

FIGURE 9. The illustration of the sensor placement. a) Measurement points of the mechano-acoustic signals (heart sounds) with respect to the heart anatomy: 1. Aortic, 2. Pulmonary, 3. Tricuspid valve, 4. Mitral valve; b) Recommended sensor placements for the heart sounds measurements (red) and the optimal FBG sensor placement (blue); c) Examples of the ECG and PCG waveforms along with the pressure in the ventriculi and the atria: The first heart sound (S1) is caused by the atrioventricular valves – Mitral (4) and Tricuspid (3). The second heart sound (S2) is caused by the semilunar valves – Aortic (1) and Pulmonary (2).

The scans were conducted using two of the most commonly used heart imaging sequences:

a) The kinematic sequence T1/T2 of the balanced echo (True Free Induction Decay Steady-State Precession (FISP) by Siemens, Erlangen, Germany) – used to assess the movement of the individual heart compartments and valves.

b) The native Phase Sensitive Inversion Recover (PSIR) sequence based on Gradient echo (GRE) T1 weighing, T1 flash with myocardial signal suppression by a variable inverse pulse. This sequence is commonly used as standard in a post-contrast manner to suppress the contrast-saturated myocardial signal. The contrast medium was not administered, the scans were performed as native, which is considered as sufficient to evaluate the usability of the triggering system (the inversion recovery (IR) time was left at the standard 270 ms).

TABLE 1. General information on the subjects tested.

Subject parameters	(N = 8)
Age (years)	40 ± 16
Females, n (%)	4 (50 %)
Males, n (%)	4 (50 %)
Height (cm)	169 ± 25
Weight (kg)	70 ± 23
Systolic blood pressure, mmHg	112 ± 33
Diastolic blood pressure, mmHg	69 ± 21

All images were obtained using a MR Magnetom Prisma 3T, Siemens (Erlangen, Germany). While this imaging system produces usable scans for clinical practice, the resulting images are often accompanied with artifacts. During the heart filling phase, individual images were obtained for each subject using a sequence adapted for that subject (region of interest, length of repetition time (TR) interval depending on heart rate). The measurement was performed within 60s in succession over two breaths, with only a different trigger device input selected between the breaths (conventional ECG and POX for an FBG-based optical system).

The individual parameters of the MR sequences used for cardiac triggering are shown in Table 2. A photograph of the measurement is shown in Fig. 10. The location of the FBG sensor on Female01 and Male01 test volunteers, respectively, is shown in red.

TABLE 2. The parameters of the MR sequences used for cardiac triggering.

Type of sequence	T1/T2 TrueFISP	PSIR
Field of view (mm)	340 × 284	350 × 263
Resolution (pixels)	208 × 174	256 × 192
Time to echo (ms)	1.4	1.5
Acquisition time (s)	10 – 18 s	11 – 17 s
Flip angle (deg)	53	2
Inversion time (ms)	-	270
Slice thickness (mm)	6	8

F. EVALUATION OF THE RESULTS

The image quality can be evaluated by means of different methods based on the specific criteria, such as the diagnostic quality of the image or its other characteristics (brightness, contrast, sharpness, etc.). It is very difficult to determine to what extent are the physical measures of image quality and

(a)

(b)

FIGURE 10. Photographs of patient instrumentation setting for triggered MRI scan: a) a female subject; b) a male subject.

observer performance correlated in clinical diagnostic work. As mentioned in [76], the relationship between fundamental physical and technical factors and image quality in diagnostic outcome is not well known. It is therefore crucial to include both, the methods taking into account the clinical and diagnostic value of the images (herein referred as subjective methods) and also the methods quantifying the technical quality of the image (herein referred as objective methods). Such objective evaluations would not provide diagnostically useful information; however, they are able to assess other quality factors that need to be considered when comparing the overall performance of the tested system.

1) OBJECTIVE EVALUATION

For the objective evaluation of the quality of the images acquired, 3 algorithms were used: 1) Blind/Referenceless Image Spatial Quality Evaluator (BRISQUE); 2) Naturalness Image Quality Evaluator (NIQE); and 3) Perception based Image Quality Evaluator (PIQE):

a) The BRISQUE algorithm was selected since it uses scene statistics of locally normalized luminance coefficients to assess the level of image quality that can be reduced due to the presence of distortions. BRISQUE is based on the calculation of the no-reference image quality score; the output value is in the range of 0-100; a smaller result value indicates better image quality.

b) The NIQE [77] and PIQE [78] algorithms are also based on the calculation of the no-reference image quality score. Again, a smaller result value indicates better image quality. NIQE uses natural scene statistics features from a corpus of natural images while the BRISQUE algorithm is trained on features received not only from natural images, but also from distorted images and human decisions about the quality of these images.

c) The PIQE algorithm is based on extracting local features to estimate the quality of the images. To imitate human behaviour, the image quality estimation is conducted using perceptually significant spatial regions [78].

2) SUBJECTIVE EVALUATION

Based on the shortcomings of the objective image evaluation methods, a subjective evaluation was performed by clinical experts. A so-called blind test was created where 10 experts evaluated the quality of the images in terms of their diagnostic quality. The group of 10 clinical experts (radiologists) was composed of 5 doctors with experience of 3 years, 5 doctors with experience of 8 years and more. Each radiologist carried out the evaluation him/herself, during the evaluation they could not discuss with each other.

IV. RESULTS OF THE PILOT PRE-CLINICAL STUDY

Example of the images intended for comparing the quality (diagnostic and image) for PSIR (Siemens) and True-FISP (Siemens) sequences are shown in Fig. 11 and Fig. 12, respectively; the rest of the images is provided in Appendix A. This is a comparison of images from the FBG-based system vs. ECG (Siemens Prisma 3T ECG reference) vs. POX (Siemens Prisma 3T Pulse Oximeter reference) for selected sequences.

The data obtained by measurement (Fig. 11) show the weighted T1 image used to evaluate myocardial enhancement after intravenous administration of the contrast agent; these are static scans.

a) In terms of phase, imaging using the FBG-based system corresponds completely to the diastole, which means it allows assessing cardiac muscle saturation in the resting phase as much as possible and it also allows visualization of the interface of the heart muscle and the heart cavity relatively sharply with a minimum of artifacts affecting the wall and the papillary muscles, despite the artifacts from the flows in the 3T device.

b) As a standard triggering tool, ECG provides a phase-correct image, that is, at the end of the diastole, a greater proportion of artifacts is evident, which may not be due to the triggering system.

c) The image created by pulse triggering is phase-shifted - there is an evident shift of the pulse wave towards the heart cycle; the artifact proportion is visible and the boundary between the artifacts from the flow and the wall of the heart compartments is blurred.

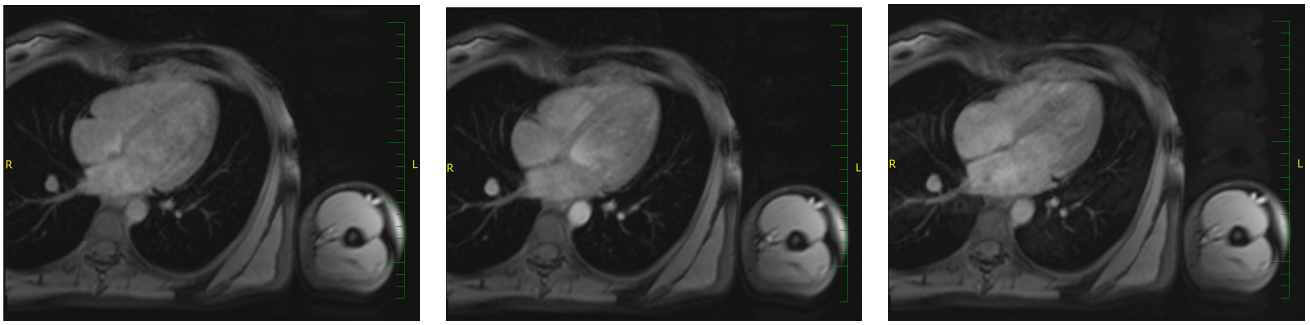

(a) (b) (c)

FIGURE 11. The resulting images (subject 1) using the PSIR sequence: a) FBG-based system; b) ECG; c) POX.

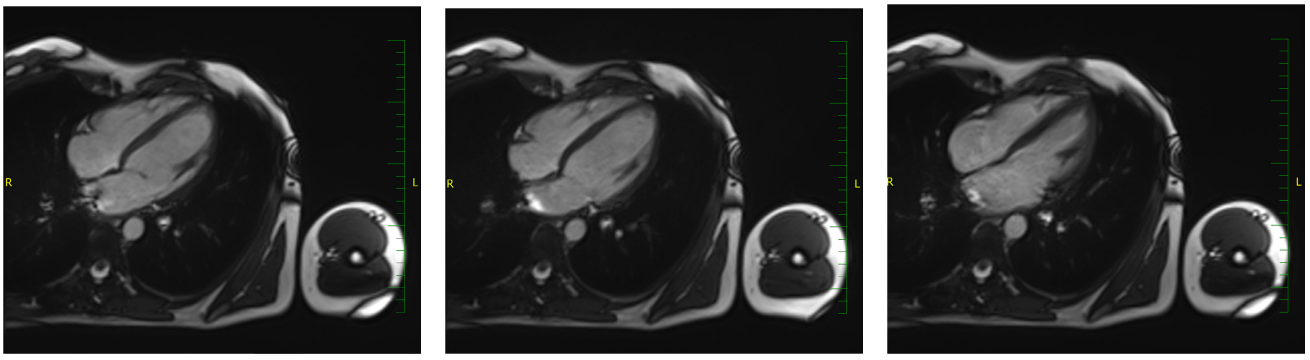

(a) (b) (c)

FIGURE 12. The resulting images (subject 2) using the TF sequence: a) FBG-based system; b) ECG; c) POX.

Figure 12 represents the results from the application of the T1/T2 sequence of the Trufisp balanced echo used to assess the movement of the heart compartments, a kinematic sequence.

a) In terms of phase, imaging using the FBG-based system corresponds completely to the diastole, which means it allows assessing the movement of the heart compartments with a sharp boundary, which affects, for example, the movement of the heart valves or the papillary muscles. The artifacts in the 3 T field are minimal, they do not interfere with the display of the ventricles; there is no interference in the display of the transition between the papillary muscle and the moving blood.
b) ECG as a standard triggering tool provides true information in the right phase of the heart function. There are slight artifacts at the interface between the papillary muscle and the flowing blood.
c) The image created by POX based triggering is phase-shifted again - the effect of the pulse wave shift towards the heart cycle and the rate of its detection is also evident here; the artifacts in the atria and at the ventricular/atrial interface are the disturbing elements of the display.

A. OBJECTIVE EVALUATION

After consultation with radiologists, clinically significant areas were selected to eliminate distortion by redundant areas. The results of objective evaluation are summarized in Tab. 3 and Tab. 4; the results that indicate the worst rating for a given algorithm/subject are highlighted in red; the results that indicate the best mean value of the rating among all tested subjects for a given algorithms are highlighted in green. These results are also depicted using Fig. 13, which shows a graphical comparison of the objective evaluation for the above-mentioned algorithms in the form of box plots for 13(a) TrueFISP and 13(b) PSIR sequences. Box plot is a simple way of representing statistical data on a plot in which a rectangle is drawn to represent the second and third quartiles, where lower and upper quartiles are shown as horizontal lines either side of the rectangle, and red vertical line inside indicates the median value.

It can be noticed that no value deviates significantly from the others so it can be stated that the technical quality of the resulting images is comparable among the tested methods. However, it is interesting to note that the low values of objective parameters (marked in red) for the PSIR sequences were distributed among all tested methods; in terms of mean values, the ECG and BCG methods outperformed the POX method. In contrast for TrueFISP sequence, the results for ECG and BCG differed – ECG method had the worst results when assessed by the BRISQUE parameter, while BCG method achieved the worst results according to PIQE parameter.

B. SUBJECTIVE EVALUATION

Within the framework of the test, the experts evaluated the above-mentioned images acquired using two different

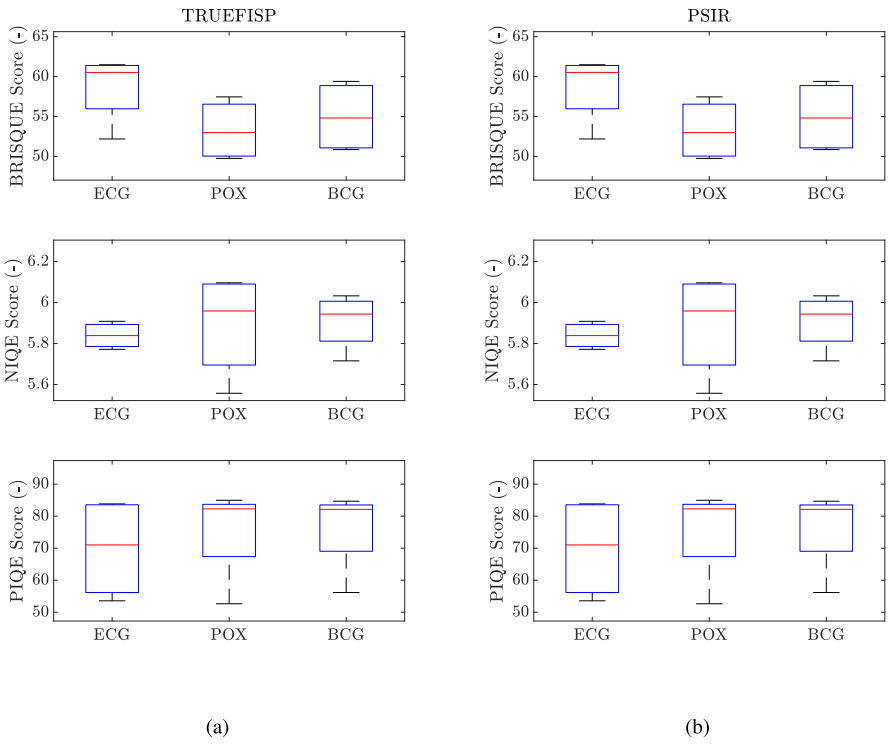

FIGURE 13. Graphical comparison of the objective evaluation in the form of BOXPLOT for a) TrueFISP; b) PSIR sequences.

TABLE 3. Summarization of the objective evaluation using TrueFISP sequence (Siemens).

Subject	ECG	POX	BCG	ECG	POX	BCG	ECG	POX	BCG
	BRISQUE			NIQE			PIQE		
2	52.1899	50.3360	51.2861	5.8780	6.0962	6.0327	83.8278	82.4357	84.6725
4	61.4847	49.7512	50.8589	5.9084	6.0846	5.9800	83.2804	84.9627	81.9288
6	59.7554	57.4620	59.4038	5.7717	5.8328	5.9077	53.5608	52.6421	56.1534
8	61.3037	55.6297	58.3477	5.7995	5.5572	5.7155	58.7699	82.1113	82.3421
Mean	**58.6834**	**53.2947**	**54.9741**	**5.8394**	**5.8927**	**5.9090**	**69.8597**	**75.5380**	**76.2742**

TABLE 4. Summarization of objective evaluation using PSIR sequence (Siemens).

Subject	ECG	POX	BCG	ECG	POX	BCG	ECG	POX	BCG
	BRISQUE			NIQE			PIQE		
1	57.1652	65.6780	67.8011	5.0773	6.0461	5.9226	84.4380	83.5372	83.6816
3	65.1133	65.7730	68.0912	5.9513	5.8215	6.2971	80.8531	84.6901	79.1312
5	66.1406	69.9604	69.9578	6.1634	5.4892	5.7667	82.1105	78.8894	80.5515
7	66.0080	64.9815	66.4981	5.7726	5.8424	5.7150	80.3866	85.5510	82.8598
Mean	**63.6068**	**66.5982**	**68.0871**	**5.7412**	**5.7998**	**5.9254**	**81.9471**	**83.1669**	**81.5560**

sequences (TrueFISP and PSIR) in combination with three different triggering methods (ECG, POX, and BCG). Therefore, each image was assessed by 10 different experts with marks ranging from 1 to 3, wherein the highest quality image was evaluated by mark 1 and the lowest quality by mark 3, see Table 5. The experts in the field did not have information about the method used for taking the image. The radiologist also "blind" to the type of triggering (i.e., ECG, POX, and BCG) that was used under each sequence - images were randomly assigned without the possibility of detecting the type of monitoring and triggering used.

Based on the results presented in Tab. 5, it can be stated that the FBG-based system achieves comparable diagnostic results in terms of diagnostic quality as the triggering methods used in clinical practice (i.e. ECG and POX). At cardiac triggering, the BCG-based system achieved slightly better results than POX, but, on the other hand, it achieved slightly worse results than the ECG-based system.

TABLE 5. Summarization of the subjective evaluation - blind test (diagnostic quality: 1 to 3 (1 best, 2 intermediate, 3 poor); average - 10 doctors).

	TrueFISP			PSIR		
Doctor performing assessment	ECG	POX	BCG	ECG	POX	BCG
1	1.7	2.0	1.8	1.8	2.0	1.9
2	1.5	1.7	1.7	1.5	2.2	1.5
3	1.3	1.5	1.4	1.8	2.3	1.7
4	1.5	1.8	1.7	1.6	2.1	1.9
5	1.5	1.4	1.5	1.4	2.0	2.1
6	1.4	1.6	1.7	1.5	2.3	1.9
7	1.6	1.7	1.9	1.5	2.1	1.7
8	1.2	1.8	1.4	1.7	1.7	1.8
9	1.3	1.5	1.7	1.9	1.9	2.1
10	1.7	1.6	1.4	1.4	1.8	1.7
Mean	**1.5**	**1.7**	**1.6**	**1.6**	**2.0**	**1.8**

V. DISCUSSION

This preclinical study has shown that the FBG-based system functions as well as the conventional systems based on ECG and POX. The comparison of these systems was carried out using both the objective and subjective evaluations and statistical analysis of the data gathered during the study. Objective methods (BRISQUE, NIQE, PIQE) of image quality evaluation were used for the evaluation of the results of this study. Based on the results assessed by these methods, the functionality of the FBG-based system against the reference ECG and POX was confirmed. However, it should be noted that these objective methods are not able to capture the diagnostic value of the images, but they are able to evaluate the fundamental physical and technical factors and thus the technical quality of the image. To evaluate also the diagnostic value of the obtained images, the team of authors also conducted a subjective blind test in this study (5 doctors and 5 radiologists). The results of this test confirmed the functionality of the proposed FBG-based system.

Based on the results of this pre-clinical cardiac triggering study, it can be expected that the proposed FBG system has the potential to shorten the examination time and to increase patient comfort. This is mainly due to simple implementation compared to the conventional ECG based system that requires several preparation procedures (shaving the hair, scrubbing the skin, etc.) to ensure optimal contact of the electrode with the skin. Of course, this expectation needs to be examined in a larger follow-up clinical study that would cover a wide spectrum of patients. The advantages and characteristic features of fiber optic sensors for MR environments include passivity in terms of power supply and electromagnetic immunity. As a result, these sensors can also be used in the presence of other electrical equipment without electrical interference, which increases patient monitoring safety.

Given the ability of the proposed system to simultaneously monitor respiratory activities [9], it would be potentially possible to detect the hyperventilation associated with the risk of developing tetanus, thus effectively preventing these conditions. However, simultaneous respiratory and pulse triggering has not been tested in this study, because the MR scanner (Prisma 3T MR scanner), which was used in this study did not allow simultaneous ECG and respiratory input for triggering. We will address this issue in our future research.

The primary disadvantages of commercially used electrical potential sensing systems include the fact that they are very difficult to shield from the eddy currents induced into the sensors/electrodes and their conductors during MR acquisition. In the case of conductive materials, eddy currents are induced not only from the gradient system but also from the high frequency - as a result, the electrodes may be heated and the subject being measured may get burnt. For electrical potential sensing systems, correct electrode application is also required to acquire a high-quality ECG waveform, i.e. correct electrode placement and proper electrode contact. Both these requirements can potentially extend the patient preparation and also elevate the risks associated with improper use of the sensing device. In contrast, the FBG-based system introduced in this article is entirely immune to electromagnetic interference and it can be employed for all currently available measuring sequences.

In the case of mass production, the price of an FBG the sensor would be based on many factors that we are currently unable to quantify. Here, we discussed the cost of a FBG sensor prototype, which includes only the cost for the Bragg grating, PDMS material, optical fiber and protection.

At this time, the cost of FBG sensor is expected to be approximately € 70 (work not included) compared to existing conventional systems based on ECG, such as SIEMENS PMU (€ 8,000) or BRAINVISION – BrainAmp ExG system (€ 40,000) [26]. The price estimation does not include the FBG interrogation unit, which costs between € 10,000 a € 20,000. This unit can be used to evaluate the results of multiple FBG sensors. Thus, the price of the system can be decreased when comprised to the department with multiple MR scanners, which is usual in the clinical practice. Table 6 shows the comparison of the tested systems with the commercially available systems for synchronous measurement utilized in the MRI of the research center CEITEC, Brno.

TABLE 6. The price comparison of monitoring systems.

Name	Price	Measured signal
BRAINVISION - BrainAmp ExG system	~ 40 000 €	ECG
Siemens PMU (PERU and PPU)	~ 8 000 €	ECG, Pulse, Respiratory
FBG system	~ 10 500 €	BCG
MRI PULSE OXIMETER 03-7500FO	~ 1 500 €	Pulse

The FBG sensor is encapsulated with the PDMS material which is resistant to most chemical substances and mechanical stress. Owing to this fact, the resulting sensor is resistant to disinfectants and is reusable by being washable and suitable for disinfecting. Therefore, the FBG sensor can be repeatedly used by proper washing and disinfecting it. Although the FBG interrogation unit, which is required for signal evaluation, is a

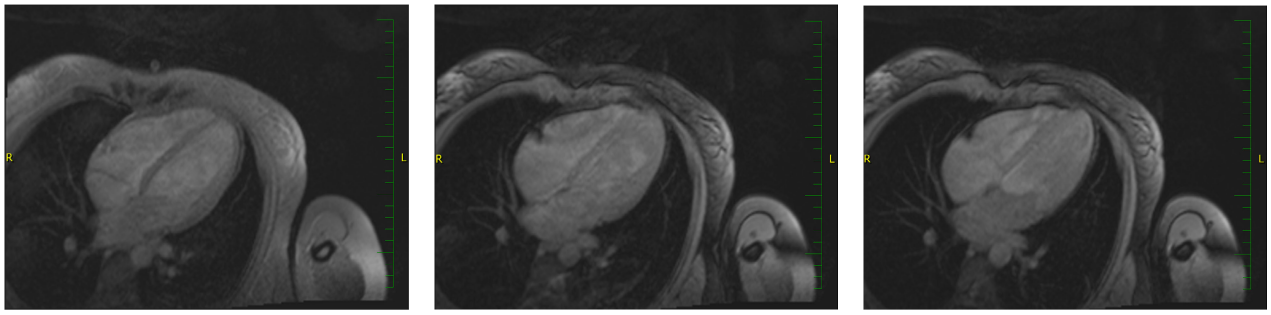

(a) (b) (c)

FIGURE 14. The resulting images (subject 3) using the PSIR sequence: a) FBG-based system; b) ECG; c) POX.

costlier device, it is possible to use the spectral evaluation approach and, using a single FBG interrogation unit, to evaluate units to dozens of sensors.

The presented concept of FBG based cardiac triggering due to its time accuracy and stability has the potential to significantly refine the trigger signal generation. The use of the proposed sensor can lead to higher image sharpness and noise reduction; thus significantly increasing the quality of acquired images. Further refinement can also be realized by considering possible alternative components to FBGuard and NI cDAQ controller. Specifically, a standalone dedicated computer-based controller unit which would measure and evaluate FBG signal directly may prove to be both computationally and financially efficient. Examples of possibly suitable computing platforms for this task are: a real-time operating system (RTOS) controller; a dedicated embedded system with ''bare metal SW'' application; or a NI cRIO platform that includes a field programmable gate array (FPGA) connected to a RTOS controller. Our next research will be focused on implementation of such highly deterministic FBG based cardiac triggering system.

VI. CONCLUSION

This pilot preclinical study investigated the suitability of the Novel FBG-based Triggering System for Cardiac MR Imaging at 3 Tesla. This first study of the fiber-optic sensors demonstrated that not only the sensor can measure the vital signs during MRI scans, but also can use these signals to properly and efficiently trigger the MR scanner to diminish the image distortion caused by body movements. Comparing the performance of the proposed system with the existing conventional triggering systems revealed equivalent performance with additional advantages. The advantages include no eddy current interference, ease of placement of the sensor on the patient's body, and sensor reusability.

APPENDIX A

The data obtained by measurement (Fig. 14) show the weighted T1 image, which is used to evaluate myocardial enhancement after intravenous administration of the contrast agent; these are static scans.

a) Imaging using the FBG-based system is in the correct phase of the heart cycle - the diastole; the artifacts at the interface between the heart wall and the flowing blood are not significant, even in the native image we can clearly distinguish the moving heart compartment and the flowing blood.
b) ECG triggering has an unambiguously higher proportion of artifacts from the flowing blood; in the left ventricle area, there is an unclear boundary between the blood and the ventricular wall, but this may be eliminated by administration of the contrast agent.
c) The image created by pulse triggering with a slight phase shift (it is no longer the end-diastole) is an indistinct boundary between the flowing blood and the left ventricular wall in the lateral wall area.

Fig. 15 shows the results from the application of the T1/T2 sequence of the Trufisp balanced echo, a kinematic sequence used to assess the movement of the heart compartments and structures.

a) Imaging using the FBG-based system - the phase of the heart cycle is with a minimal shift compared to the ECG trigged image; it is not a pure end-diastole, there is a good anatomical correlation of the heart compartments with a clear boundary, the artifacts are apparent at the interface between the right ventricle and the atrium, the rendering of the papillary muscles is excellent even in comparison with the ECG image.
b) ECG as a standard triggering tool provides good phase-displayed information; slight artifacts are apparent at the interface between the papillary muscle and the flowing blood, the rendering of the papillary muscles is worse.
c) The image created by pulse triggering is also with a minimal shift in the phase of the heart cycle; the artifacts in the atria are more prominent.

The data obtained by measurement (Fig. 16) show the weighted T1 image.

a) Imaging using the FBG-based system - the image corresponds to the end-diastole; in this subject, there are more prominent artifacts from the flow, but the

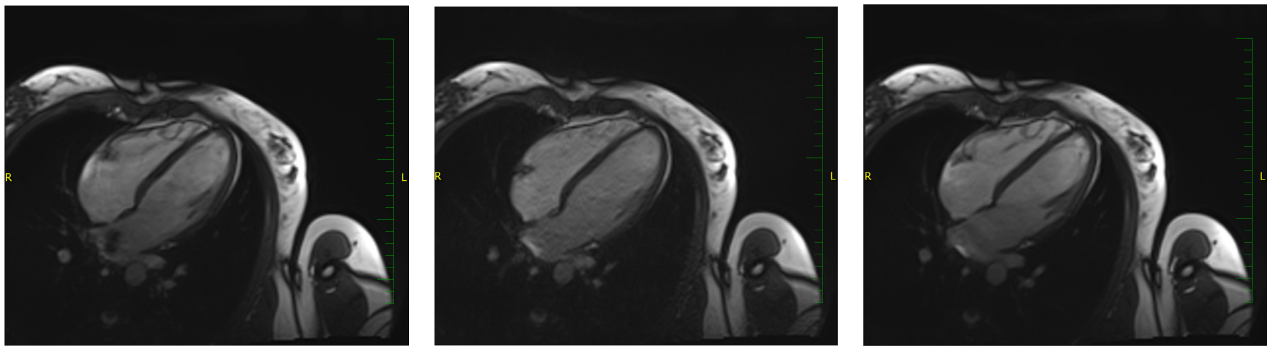

(a) (b) (c)

FIGURE 15. The resulting images (subject 4) using the TF sequence: a) FBG-based system; b) ECG; c) POX.

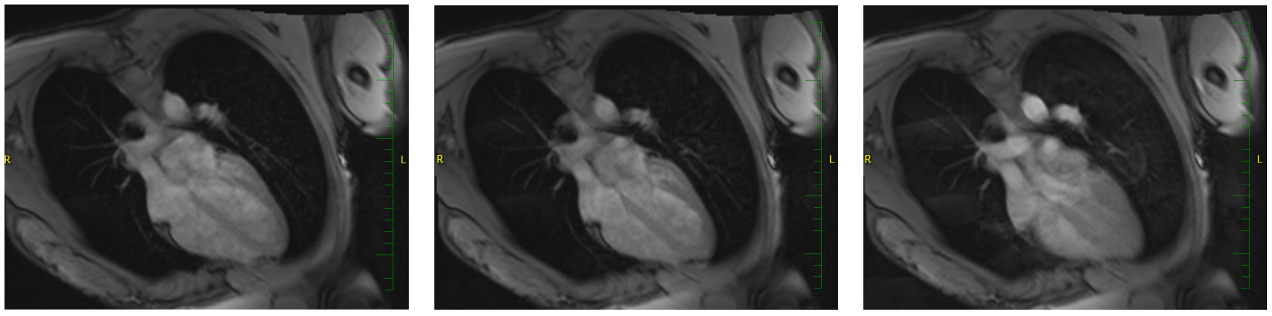

(a) (b) (c)

FIGURE 16. The resulting images (subject 5) using the PSIR sequence: a) FBG-based system; b) ECG; c) POX.

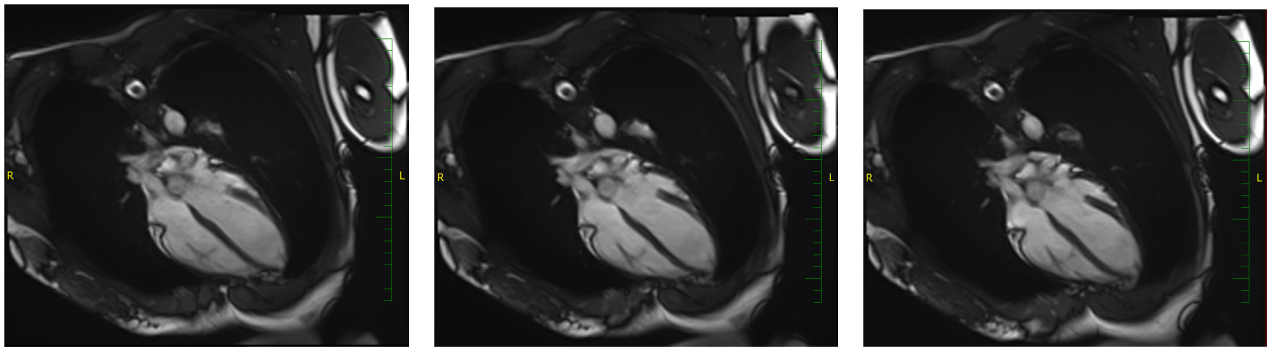

(a) (b) (c)

FIGURE 17. The resulting images (subject 6) using the TF sequence: a) FBG-based system; b) ECG; c) POX.

boundary of the anatomically stable structures is still clearly visible.

b) ECG triggering corresponds to the phase of the heart cycle; the proportion of artifacts, particularly in the left atrium and the left ventricle, is significant.

c) The image created by pulse triggering is made with a disturbing phase shift, the heart is already in the stage of the presystole (up to the systole), the proportion of artifacts from the blood flow is significant, there is a very poorly detectable boundary between the solid and liquid tissue.

Fig. 17 represents the results from the application of the T1/T2 sequence of the Trufisp sequence.

a) Imaging using the FBG-based system - the phase of the heart cycle is phase accurate, the boundaries of the anatomical structures are sharp, the artifacts are an obstacle in the atrium and right ventricle area and they do not distort the movement of the left ventricle

b) ECG triggering is phase identical to BCG triggering, the image sharpness is very similar, the proportion of artifacts is comparable, the image is not diagnostically more accurate than BCG triggering.

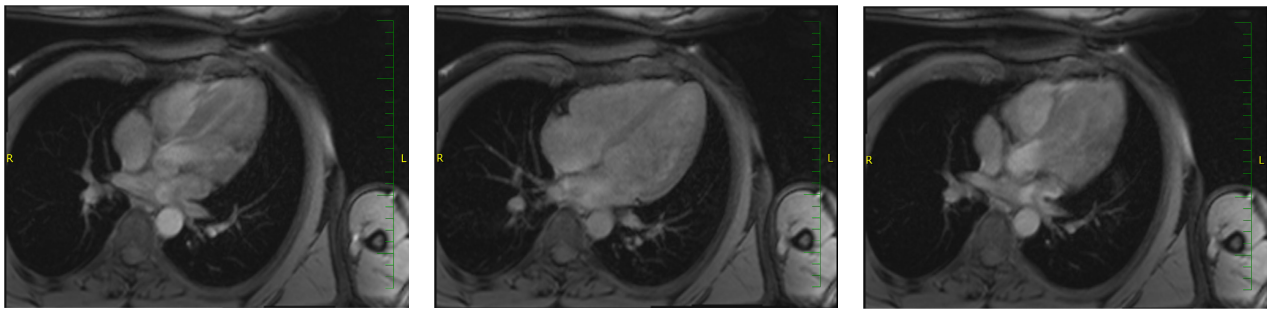

(a) (b) (c)

FIGURE 18. The resulting images (subject 7) using the PSIR sequence: a) FBG-based system; b) ECG; c) POX.

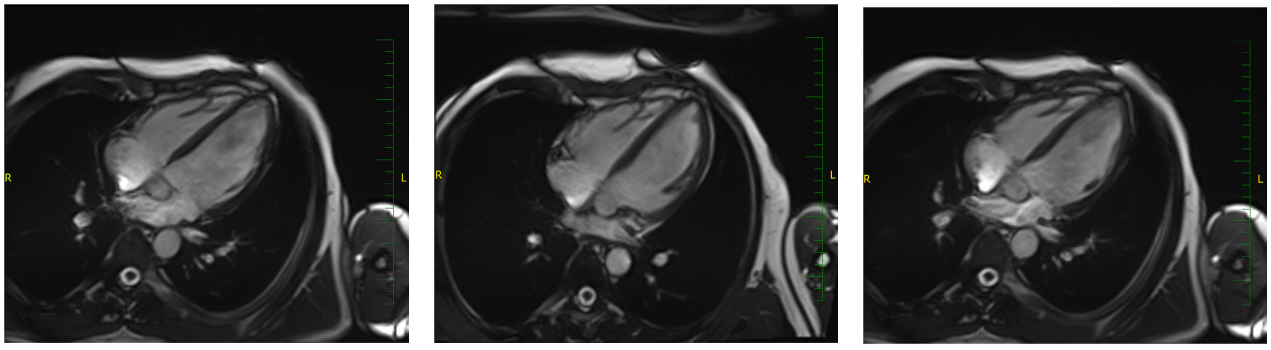

(a) (b) (c)

FIGURE 19. The resulting images (subject 8) using the TF sequence: a) FBG-based system; b) ECG; c) POX.

c) The image created by pulse triggering it is without a significant phase shift, even in this triggering system, the proportion of blood flow artifacts is evident in the 3T device.

The data in Fig. 18 show the weighted T1 image.

a) Imaging using the FBG-based system - the image does not correspond to the end-diastole, there is a visible phase shift to the presystole, there is a significant proportion of artifacts of the flowing blood, but the boundaries of the anatomical compartments are clear.
b) As a standard in this subject, ECG triggering provides infiltration in the end-diastole, the boundaries of the anatomical compartments and the flowing blood are relatively well apparent, apart from the lateral segment of the apex and the middle part of the left ventricle.
c) The image created by pulse triggering is with a significant phase shift to the systolic contraction, there is no clear anatomical boundary of the heart compartments, the proportion of artifacts of the flowing blood is high.

Fig. 19 shows the results from the application of the kinematic Trufisp sequence.

a) Imaging using the FBG-based system - the phase of the heart cycle corresponds to the end-diastole, the widest dimension of the left ventricle of all images acquired using different triggering techniques is visible, there is a sharp transition of the solid ventricular wall and the flowing blood, the rendering of the papillary muscles is good, without artifacts.
b) ECG triggering has a minimal phase shift outside the end-diastole, there is an apparent artifact at the interface between the left ventricular wall and the papillary muscle, there is no sharp boundary between the solid heart compartments and the flowing fluid.
c) The image created by pulse triggering it is without a significant phase shift, the structure of the papillary muscles is not well rendered, there is a higher proportion of artifacts from the movement of the valves and the flowing blood.

ETHICS STATEMENT

Ref. No.: EKV-2019-098 Project Title: Fiber Bragg grating system for vital function monitoring and triggering in strong magnetic field environment (MRI), 1374/2019, Investigator: Petr Kudlicka, Organizational Unit: CEITEC The Research Ethics Committee of Masaryk University has reviewed the application to conduct the research project as specified above and on December 2019 the Committee has approved this project to be conducted.

REFERENCES

[1] R. Ehman, M. McNamara, M. Pallack, H. Hricak, and C. Higgins, "Magnetic resonance imaging with respiratory gating: Techniques and advantages," *Amer. J. Roentgenol.*, vol. 143, no. 6, pp. 1175–1182, Dec. 1984.
[2] C. E. Lewis, F. S. Prato, D. J. Drost, and R. L. Nicholson, "Comparison of respiratory triggering and gating techniques for the removal of respiratory artifacts in MR imaging.," *Radiology*, vol. 160, no. 3, pp. 803–810, Sep. 1986.

[3] D. Wenz, A. M. Nagel, J. Lott, A. Kuehne, S. C. Niesporek, and T. Niendorf, "*In vivo* potassium MRI of the human heart," *Magn. Reson. Med.*, vol. 83, no. 1, pp. 203–213, Jan. 2020.

[4] D.-M. Koh, M. Blackledge, A. R. Padhani, T. Takahara, T. C. Kwee, M. O. Leach, and D. J. Collins, "Whole-body diffusion-weighted MRI: Tips, tricks, and pitfalls," *Amer. J. Roentgenol.*, vol. 199, no. 2, pp. 252–262, Aug. 2012.

[5] C. Michel, C. Marcus, J.-L. Bigot, N. Henon, and B. Menanteau, "Fat suppression in MR imaging: Advantages and pitfalls," *Feuillets de Radiologie*, vol. 44, pp. 357–365, 2004.

[6] M. Zaitsev, J. Maclaren, and M. Herbst, "Motion artifacts in MRI: A complex problem with many partial solutions," *J. Magn. Reson. Imag.*, vol. 42, no. 4, pp. 887–901, Oct. 2015.

[7] E. K. Outwater, R. Blasbalg, E. S. Siegelman, and M. Vala, "Detection of lipid in abdominal tissues with opposed-phase gradient-echo images at 1.5 T: Techniques and diagnostic importance," *RadioGraphics*, vol. 18, no. 6, pp. 1465–1480, Nov. 1998.

[8] P. Storey, Q. Chen, W. Li, R. R. Edelman, and P. V. Prasad, "Band artifacts due to bulk motion," *Magn. Reson. Med.*, vol. 48, no. 6, pp. 1028–1036, Dec. 2002.

[9] F. C. Moreton, K. A. Dani, C. Goutcher, K. O'Hare, and K. W. Muir, "Respiratory challenge MRI: Practical aspects," *NeuroImage: Clin.*, vol. 11, pp. 667–677, 2016.

[10] Z. Sun, "Multislice CT angiography in cardiac imaging: Prospective ECG-gating or retrospective ECG-gating?" *Biomed. Imag. Intervent. J.*, vol. 6, no. 1, p. e4, Jan. 2010.

[11] P. Velankar, K. Chaikriangkrai, N. Dewal, S. K. Bala, B. Elferjani, S. Alchalabi, and S. M. Chang, "Prognostic performance of prospective versus retrospective electrocardiographic gating in coronary computed tomographic angiography," *Texas Heart Inst. J.*, vol. 45, no. 4, pp. 214–220, Aug. 2018.

[12] D. Gopalan, "Right heart on multidetector CT," *Brit. J. Radiol.*, vol. 84, no. 3, pp. S306–S323, Dec. 2011.

[13] P. Lanzer, C. Barta, E. H. Botvinick, H. U. Wiesendanger, G. Modin, and C. B. Higgins, "ECG-synchronized cardiac MR imaging: Method and evaluation," *Radiology*, vol. 155, no. 3, pp. 681–686, Jun. 1985.

[14] B. A. Herzog, L. Husmann, N. Burkhard, O. Gaemperli, I. Valenta, F. Tatsugami, C. A. Wyss, U. Landmesser, and P. A. Kaufmann, "Accuracy of low-dose computed tomography coronary angiography using prospective electrocardiogram-triggering: First clinical experience," *Eur. Heart J.*, vol. 29, no. 24, pp. 3037–3042, Dec. 2008.

[15] J. Nedoma, S. Kepak, M. Fajkus, J. Cubik, P. Siska, R. Martinek, and P. Krupa, "Magnetic resonance imaging compatible non-invasive fibre-optic sensors based on the Bragg gratings and interferometers in the application of monitoring heart and respiration rate of the human body: A comparative study," *Sensors*, vol. 18, no. 11, p. 3713, Oct. 2018.

[16] J. Nedoma, M. Fajkus, R. Martinek, and H. Nazeran, "Vital sign monitoring and cardiac triggering at 1.5 tesla: A practical solution by an MR-ballistocardiography fiber-optic sensor," *Sensors*, vol. 19, no. 3, p. 470, Jan. 2019.

[17] M. Fajkus, J. Nedoma, R. Martinek, J. Brablik, J. Vanus, M. Novak, S. Zabka, V. Vasinek, P. Hanzlikova, and L. Vojtisek, "MR fully compatible and safe FBG breathing sensor: A practical solution for respiratory triggering," *IEEE Access*, vol. 7, pp. 123013–123025, 2019.

[18] J. Nedoma, M. Fajkus, and R. Martinek, "Fiber-optic breath sensors: A comparison study," *J. Biomimetics, Biomater. Biomed. Eng.*, vol. 40, pp. 56–63, Feb. 2019.

[19] J. Nedoma, M. Fajkus, J. Cubik, S. Kepak, R. Martinek, J. Vanus, and R. Jaros, "SMART medical polydimethylsiloxane for monitoring vital signs of the human body," in *Proc. IEEE 20th Int. Conf. e-Health Netw., Appl. Services (Healthcom)*, Sep. 2018, pp. 1–4.

[20] J. Nedoma, M. Fajkus, J. Jargus, R. Martinek, V. Vasinek, K. Witas, and J. Vanus, "Analysis of encapsulation the fiber Bragg sensors for biomedical applications," in *Fiber Optic Sensors and Applications XV*, H. H. Du, A. Mendez, and C. S. Baldwin, Eds. Bellingham, WA, USA: SPIE, 2018.

[21] M. Fajkus, J. Nedoma, R. Martinek, V. Vasinek, H. Nazeran, and P. Siska, "A non-invasive multichannel hybrid fiber-optic sensor system for vital sign monitoring," *Sensors*, vol. 17, no. 12, p. 111, Jan. 2017.

[22] T. Niendorf, L. Winter, and T. Frauenrath, "Electrocardiogram in an MRI environment: Clinical needs, practical considerations, safety implications, technical solutions and future directions," in *Advances in Electrocardiograms - Methods and Analysis*. Rijeka, Croatia: InTech, 2012.

[23] L. Axel and M. A. Toms, "Clinical cardiac magnetic resonance imaging techniques," in *Contemporary Cardiology*. New York, NY, USA: Springer 2019, pp. 17–50.

[24] N. Spicher, M. Kukuk, S. Maderwald, and M. E. Ladd, "Initial evaluation of prospective cardiac triggering using photoplethysmography signals recorded with a video camera compared to pulse oximetry and electrocardiography at 7T MRI," *Biomed. Eng. OnLine*, vol. 15, no. 1, p. 126, Dec. 2016.

[25] N. Spicher, "Cardiac activity measurement from video signals of the human skin in ultrahigh-field magnetic resonance imaging," in *Informatik*, H. C. Mayr and M. Pinzger, Eds. Bonn, Germany: Gesellschaft fur Informatik e.V., 2016, pp. 1999–2004.

[26] R. Martinek, J. Brablik, J. Kolarik, M. Ladrova, J. Nedoma, R. Jaros, L. Soustek, R. Kahankova, M. Fajkus, L. Vojtisek, P. Hanzlikova, and P. Krupa, "A low-cost system for seismocardiography-based cardiac triggering: A practical solution for cardiovascular magnetic resonance imaging at 3 tesla," *IEEE Access*, vol. 7, pp. 118608–118629, 2019.

[27] A. Dinh, Y. Choi, and S.-B. Ko, "A heart rate sensor based on seismocardiography for vital sign monitoring systems," in *Proc. 24th Can. Conf. Electr. Comput. Engineering(CCECE)*, May 2011, pp. 665–668.

[28] M. Jerosch-Herold, J. Zanetti, H. Merkle, L. Poliac, H. Huang, A. Mansoor, F. Zhao, and N. Wilke, "The seismocardiogram as magnetic-field-compatible alternative to the electrocardiogram for cardiac stress monitoring," *Int. J. Cardiac Imag.*, vol. 15, no. 6, pp. 523–531, 1999.

[29] L. Dziuda, "Fiber-optic sensors for monitoring patient physiological parameters: A review of applicable technologies and relevance to use during magnetic resonance imaging procedures," *J. Biomed. Opt.*, vol. 20, no. 1, 2015, Art. no. 010901.

[30] J. G. V. Teixeira, I. T. Leite, S. Silva, and O. Frazão, "Advanced fiber-optic acoustic sensors," *Photon. Sensors*, vol. 4, no. 3, pp. 198–208, Sep. 2014.

[31] L. Dziuda, M. Krej, and F. W. Skibniewski, "Fiber Bragg grating strain sensor incorporated to monitor patient vital signs during MRI," *IEEE Sensors J.*, vol. 13, no. 12, pp. 4986–4991, Dec. 2013.

[32] M. Krej, L. Dziuda, and F. W. Skibniewski, "A method of detecting heartbeat locations in the ballistocardiographic signal from the fiber-optic vital signs sensor," *IEEE J. Biomed. Health Informat.*, vol. 19, no. 4, pp. 1443–1450, Jul. 2015.

[33] Y. Yao, S. Shin, A. Mousavi, C.-S. Kim, L. Xu, R. Mukkamala, and J.-O. Hahn, "Unobtrusive estimation of cardiovascular parameters with limb ballistocardiography," *Sensors*, vol. 19, no. 13, p. 2922, Jul. 2019.

[34] O. T. Inan, D. Park, L. Giovangrandi, and G. T. A. Kovacs, "Noninvasive measurement of physiological signals on a modified home bathroom scale," *IEEE Trans. Biomed. Eng.*, vol. 59, no. 8, pp. 2137–2143, Aug. 2012.

[35] P. Roriz, L. Carvalho, O. Frazão, J. Santos, and J. Simões, "From conventional sensors to fibre optic sensors for strain and force measurements in biomechanics applications: A review," *J. Biomech.*, vol. 47, no. 6, pp. 1251–1261, 2014.

[36] Ł.Dziuda, "Fiber-optic sensors for monitoring patient physiological parameters," *J. Biomed. Opt.*, vol. 20, no. 01, pp. 1–23, Jan. 2015. [Online]. Available: https://www.spiedigitallibrary.org/journals/journal-of-biomedical-optics/volume-20/issue-01/010901/Fiber-optic-sensors-for-monitoring-patient-physiol ogical-parameters–a/10.1117/1.JBO.20.1.010901.full

[37] K. Chethana, A. S. Guru Prasad, S. N. Omkar, and S. Asokan, "Fiber Bragg grating sensor based device for simultaneous measurement of respiratory and cardiac activities," *J. Biophoton.*, vol. 10, no. 2, pp. 278–285, Feb. 2017, doi: 10.1002/jbio.201500268.

[38] L. Dziuda, F. W. Skibniewski, M. Krej, and J. Lewandowski, "Monitoring respiration and cardiac activity using fiber Bragg grating-based sensor," *IEEE Trans. Biomed. Eng.*, vol. 59, no. 7, pp. 1934–1942, Jul. 2012. [Online]. Available: http://ieeexplore.ieee.org/document/6183490/

[39] M. Fajkus, J. Nedoma, R. Martinek, V. Vasinek, H. Nazeran, and P. Siska, "A non-invasive multichannel hybrid fiber-optic sensor system for vital sign monitoring," *Sensors*, vol. 17, no. 12, p. 111, 2017. [Online]. Available: http://www.mdpi.com/1424-8220/17/1/111

[40] Ł. Dziuda, F. W. Skibniewski, M. Krej, and P. M. Baran, "Fiber Bragg grating-based sensor for monitoring respiration and heart activity during magnetic resonance imaging examinations," *J. Biomed. Opt.*, vol. 18, no. 5, pp. 278–285, 2013. [Online]. Available: https://doi.org/10.1117/1.JBO.18.5.057006

[41] D. L. Presti, C. Romano, C. Massaroni, J. D'Abbraccio, L. Massari, M. A. Caponero, C. M. Oddo, D. Formica, and E. Schena, "Cardio-respiratory monitoring in archery using a smart textile based on flexible fiber Bragg grating sensors," *Sensors*, vol. 19, no. 16, p. 3581, 2019. [Online]. Available: https://www.mdpi.com/1424-8220/19/16/3581

[42] Y. Haseda, J. Bonefacino, H.-Y. Tam, S. Chino, S. Koyama, and H. Ishizawa, "Measurement of pulse wave signals and blood pressure by a plastic optical fiber FBG sensor," *Sensors*, vol. 19, no. 23, p. 5088, 2019. [Online]. Available: https://www.mdpi.com/1424-8220/19/23/5088

[43] C. Massaroni, M. Zaltieri, D. L. Presti, A. Nicolò, D. Tosi, E. Schena, "Fiber Bragg grating sensors for cardiorespiratory monitoring," *IEEE Sensors J.*, early access, Apr. 20, 2020. [Online]. Available: https://ieeexplore.ieee.org/document/9072092/, doi: 10.1109/JSEN.2020.2988692.

[44] D. Lo Presti, C. Massaroni, J. D'Abbraccio, L. Massari, M. Caponero, U. G. Longo, D. Formica, C. M. Oddo, and E. Schena, "Wearable system based on flexible FBG for respiratory and cardiac monitoring," *IEEE Sensors J.*, vol. 19, no. 17, pp. 7391–7398, Sep. 2019. [Online]. Available: https://ieeexplore.ieee.org/document/8713482/

[45] C. Massaroni, P. Saccomandi, D. Formica, D. Lo Presti, M. A. Caponero, G. Di Tomaso, F. Giurazza, M. Muto, and E. Schena, "Design and feasibility assessment of a magnetic resonance-compatible smart textile based on fiber Bragg grating sensors for respiratory monitoring," *IEEE Sensors J.*, vol. 16, no. 22, pp. 8103–8110, Nov. 2016. [Online]. Available: http://ieeexplore.ieee.org/document/7562517/

[46] F. Taffoni, D. Formica, P. Saccomandi, G. Pino, and E. Schena, "Optical fiber-based MR-compatible sensors for medical applications: An Overview," *Sensors*, vol. 13, no. 10, pp. 14105–14120, 2013. [Online]. Available: http://www.mdpi.com/1424-8220/13/10/14105

[47] D. L. Presti, C. Massaroni, D. Formica, P. Saccomandi, F. Giurazza, M. A. Caponero, and E. Schena, "Smart textile based on 12 fiber Bragg gratings array for vital signs monitoring," *IEEE Sensors J.*, vol. 17, no. 18, pp. 6037–6043, Sep. 2017. [Online]. Available: http://ieeexplore.ieee.org/document/7990494/

[48] D. W. Chakeres, A. Kangarlu, H. Boudoulas, and D. C. Young, "Effect of static magnetic field exposure of up to 8 tesla on sequential human vital sign measurements," *J. Magn. Reson. Imag.*, vol. 18, no. 3, pp. 346–352, Sep. 2003.

[49] V. Mornstein, I. Hrazdira, and A. Bourek, *Lékařská Fyzika a Informatika: (se zaměřením na Zubní Lékařství)*. Brno, Czech Republic: Neptun, 2007.

[50] K. S. N. Gerald and M. Pohost, *Handbook of Cardiovascular Magnetic Resonance Imaging*, vol. 60, 1st ed. Boca Raton, FL, USA: CRC Press, 2006.

[51] J. W. Krug and G. Rose, "Magnetohydrodynamic distortions of the ECG in different MR scanner configurations," in *Proc. Comput. Cardiol.*, Sep. 2011, pp. 769–772.

[52] A. C. Larson, P. Kellman, A. Arai, G. A. Hirsch, E. McVeigh, D. Li, and O. P. Simonetti, "Preliminary investigation of respiratory self-gating for free-breathing segmented cine MRI," *Magn. Reson. Med.*, vol. 53, no. 1, pp. 159–168, 2004.

[53] B. Hiba, N. Richard, M. Janier, and P. Croisille, "Cardiac and respiratory double self-gated cine MRI in the mouse at 7 t," *Magn. Reson. Med.*, vol. 55, no. 3, pp. 506–513, 2006.

[54] A. C. Larson, R. D. White, G. Laub, E. R. McVeigh, D. Li, and O. P. Simonetti, "Self-gated cardiac cine MRI," *Magn. Reson. Med.*, vol. 51, no. 1, pp. 93–102, 2003.

[55] M. Becker, T. Frauenrath, F. Hezel, G. A. Krombach, U. Kremer, B. Koppers, C. Butenweg, A. Goemmel, J. F. Utting, J. Schulz-Menger, and T. Niendorf, "Comparison of left ventricular function assessment using phonocardiogram- and electrocardiogram-triggered 2D SSFP CINE MR imaging at 1.5 t and 3.0 T," *Eur. Radiol.*, vol. 20, no. 6, pp. 1344–1355, Jun. 2010.

[56] S. Maderwald, S. Orzada, and Z. Lin, "7 tesla cardiac imaging with a phonocardiogram trigger device," in *Proc. SAG Developement-Proc. Intl. Soc. Mag. Reson. Med*, vol. 19, 2011, p. 1322.

[57] T. Frauenrath, S. Kozerke, and P. Boesiger, "Cardiac gating free of interference with electro-magnetic fields at 1.5 T, 3.0 T and 7.0 T," in *Proc. Annu. meeting Int. Soc. Magn. Res. Med*, vol. 16, 2008, p. 207.

[58] K. Nassenstein, S. Orzada, L. Haering, A. Czylwik, M. Zenge, H. Eberle, T. Schlosser, O. Bruder, E. Müller, M. E. Ladd, and S. Maderwald, "Cardiac MRI: Evaluation of phonocardiogram-gated cine imaging for the assessment of global und regional left ventricular function in clinical routine," *Eur. Radiol.*, vol. 22, no. 3, pp. 559–568, Mar. 2012.

[59] T. Frauenrath, T. Niendorf, and M. Kob, "Acoustic method for synchronization of magnetic resonance imaging (MRI)," *Acta Acustica United Acustica*, vol. 94, no. 1, pp. 148–155, 2008.

[60] T. Frauenrath, F. Hezel, W. Renz, T. D. G. d'Orth, M. Dieringer, F. von Knobelsdorff-Brenkenhoff, M. Prothmann, J. Schulz-Menger, and T. Niendorf, "Acoustic cardiac triggering: A practical solution for synchronization and gating of cardiovascular magnetic resonance at 7 tesla," *J. Cardiovascular Magn. Reson.*, vol. 12, no. 1, Dec. 2010.

[61] A. G. Leal-Junior, C. R. Díaz, C. Leitão, M. J. Pontes, C. Marques, and A. Frizera, "Polymer optical fiber-based sensor for simultaneous measurement of breath and heart rate under dynamic movements," *Opt. Laser Technol.*, vol. 109, pp. 429–436, Jan. 2019.

[62] M. Ciocchetti, C. Massaroni, P. Saccomandi, M. Caponero, A. Polimadei, D. Formica, and E. Schena, "Smart textile based on fiber Bragg grating sensors for respiratory monitoring: Design and preliminary trials," *Biosensors*, vol. 5, no. 3, pp. 602–615, Sep. 2015.

[63] A. C. S. Brau, C. T. Wheeler, L. W. Hedlund, and G. A. Johnson, "Fiber-optic stethoscope: A cardiac monitoring and gating system for magnetic resonance microscopy," *Magn. Reson. Med.*, vol. 47, no. 2, pp. 314–321, Feb. 2002.

[64] A. Rengle, L. Baboi, H. Saint-Jalmes, R. Sablong, and O. Beuf, "Optical cardiac and respiratory device for synchronized MRI on small animal," in *Proc. 29th Annu. Int. Conf. IEEE Eng. Med. Biol. Soc.*, Aug. 2007, pp. 2046–2049.

[65] R. Sablong, A. Rengle, A. Ramgolam, H. Saint-Jalmes, and O. Beuf, "An optical fiber-based gating device for prospective mouse cardiac MRI," *IEEE Trans. Biomed. Eng.*, vol. 61, no. 1, pp. 162–170, Jan. 2014.

[66] N. J. Fendinger, "Polydimethylsiloxane (PDMS): Environmental fate and effects," in *Organosilicon Chemistry Set*. Weinheim, Germany: Wiley-VCH, 2005, pp. 626–638.

[67] E. Vorathin, Z. M. Hafizi, N. Ismail, and M. Loman, "Review of high sensitivity fibre-optic pressure sensors for low pressure sensing," *Opt. Laser Technol.*, vol. 121, Jan. 2020, Art. no. 105841.

[68] A. D. Kersey, M. A. Davis, H. J. Patrick, M. LeBlanc, K. P. Koo, C. G. Askins, M. A. Putnam, and E. J. Friebele, "Fiber grating sensors," *J. Lightw. Technol.*, vol. 15, no. 8, pp. 1442–1462, Aug. 1997.

[69] I. T. Union, *G.652: Characteristics a Single-Mode Opt. Fibre Cable*, document E 41163, Telecommunication Standardization Sector of ITU-T, Nov. 2016. [Online]. Available: https://www.itu.int/rec/T-REC-G.652-201611-I/en?fbclid=IwAR16ZFWEvJ6AhASn9pwpbSB7oBPJCgddG-fDuKxDcj2jZuwZN72Vfu5Enzw

[70] R. N. Palchesko, L. Zhang, Y. Sun, and A. W. Feinberg, "Development of polydimethylsiloxane substrates with tunable elastic modulus to study cell mechanobiology in muscle and nerve," *PLoS ONE*, vol. 7, no. 12, Dec. 2012, Art. no. e51499.

[71] J. Nedoma, M. Fajkus, L. Bednarek, J. Frnda, J. Zavadil, and V. Vasinek, "Encapsulation of FBG sensor into the PDMS and its effect on spectral and temperature characteristics," *Adv. Electr. Electron. Eng.*, vol. 14, no. 4, Nov. 2016.

[72] D. Tosi, "Review and analysis of peak tracking techniques for fiber Bragg grating sensors," *Sensors*, vol. 17, no. 10, p. 2368, 2017. [Online]. Available: http://www.mdpi.com/1424-8220/17/10/2368

[73] C. Elliott, V. Vijayakumar, W. Zink, and R. Hansen, "National instruments LabVIEW: A programming environment for laboratory automation and measurement," *J. Assoc. Lab. Autom.*, vol. 12, no. 1, pp. 17–24, Feb. 2007.

[74] I. Sadek, J. Biswas, and B. Abdulrazak, "Ballistocardiogram signal processing: A review," *Health Inf. Sci. Syst.*, vol. 7, no. 1, Dec. 2019.

[75] B. Karnath and W. Thornton, "Auscultation of the heart," *Hospital Physician*, vol. 38, no. 9, pp. 39–45, 2002.

[76] L. G. M Nsson, "Methods for the evaluation of image quality: A review," *Radiat. Protection Dosimetry*, vol. 90, no. 1, pp. 89–99, Aug. 2000.

[77] A. Mittal, R. Soundararajan, and A. C. Bovik, "Making a 'Completely blind' image quality analyzer," *IEEE Signal Process. Lett.*, vol. 20, no. 3, pp. 209–212, Mar. 2013.

[78] V. N, P. D, M. Chandrasekhar Bh, S. S. Channappayya, and S. S. Medasani, "Blind image quality evaluation using perception based features," in *Proc. 21st Nat. Conf. Commun. (NCC)*, Feb. 2015, pp. 1–6.

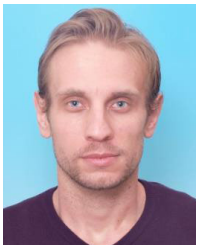

JAN NEDOMA was born in Czech Republic, in 1988. He received the master's degree in information and communication technology from the VŠB–Technical University of Ostrava, in 2014. Since 2014, he has been working as a Research Fellow. In 2017, he successfully defended his dissertation thesis and works as an Assistant Professor at the VŠB–Technical University of Ostrava. His current research interests include fiber-optic sensors in traffic, civil engineering, and biomedical applications. He has more than 135 journal articles and conference papers (author H-index: nine without self-citations) in his research areas and eight valid patents.

RADEK MARTINEK (Member, IEEE) was born in Czech Republic, in 1984. He received the master's degree in information and communication technology from the VŠB–Technical University of Ostrava, in 2009. Since 2012, he has been working as a Research Fellow. In 2014, he successfully defended his dissertation thesis titled The Use of Complex Adaptive Methods of Signal Processing for Refining the Diagnostic Quality of the Abdominal Fetal Electrocardiogram. He became an Associate Professor in technical cybernetics, in 2017, after defending the habilitation thesis titled Design and Optimization of Adaptive Systems for Applications of Technical Cybernetics and Biomedical Engineering Based on Virtual Instrumentation. He has been working as an Associate Professor at the VŠB–Technical University of Ostrava, since 2017. His current research interests include digital signal processing (linear and adaptive filtering, soft computing-artificial intelligence and adaptive fuzzy systems, non-adaptive methods, biological signal processing, and digital processing of speech signals), wireless communications (software-defined radio), and power quality improvement. He has more than 200 journal articles and conference papers in his research areas.

MARCEL FAJKUS was born in Czech Republic, in 1987. He has been working as an Assistant Professor at the VŠB-TUO Technical University of Ostrava, since 2016. His current research interests include fiber Bragg sensors and distributed systems in traffic, civil engineering, and biomedical applications.

JINDRICH BRABLIK was born in 1991. He graduated from the Faculty of Electrical Engineering and Computer Science, VŠB–Technical University of Ostrava. He received the bachelor's degree in biomedical technician and the master's degree information and control systems. He is currently pursuing the Ph.D. degree in technical cybernetics with the VŠB–Technical University of Ostrava. He focuses on virtual instrumentation and signal processing of physiological signals at the VŠB–Technical University of Ostrava.

RADANA KAHANKOVA was born in Opava, Czech Republic, in 1991. She received the master's and Ph.D. degrees from the Department of Cybernetics and Biomedical Engineering, VŠB–Technical University of Ostrava, in 2016 and 2019, respectively. Her current research interests include improving the quality of electronic fetal monitoring and magnetic resonance imaging.

MICHAEL FRIDRICH was born in Trutnov, Czech Republic, in 1995. He received the bachelor's and master's degrees in information and communication technology from the VŠB–Technical University of Ostrava, in 2017 and 2019, respectively, where he is currently pursuing the Ph.D. degree. During his doctoral studies, he focuses on fiber Bragg sensors and distributed systems in transportation, construction, and biomedical applications.

MICHAL KOSTELANSKY was born in Hodonín, Czech Republic, in 1993. He received the bachelor's and master's degrees in information technologies from the Department of Information and Communications Technologies, Faculty of Electrical Engineering and Computer Science, VŠB–Technical University of Ostrava, in 2016 and 2019, respectively, where he is currently pursuing the Ph.D. degree. His current research interests include fiber-optic sensors predominantly in biomedical applications, traffic, and civil engineering.

PAVLA HANZLIKOVA is currently working at the Clinic of Imaging Methods of Faculty Hospital, Ostrava, and deals with interventional neuroradiology, MR spectroscopy, and interventional applications of 3-D image.

LUBOMIR VOJTISEK received the Ph.D. degree in measurement from the Faculty of Electrical Engineering and Information Technology, Slovak University of Technology. He is currently a Researcher and a Technical Specialist Member of the Multimodal and Functional Neuroimaging Research Group. He works as Postdoctoral Research Fellow.

KHOSROW BEHBEHANI (Fellow, IEEE) received the B.S. degree in mechanical engineering from Louisiana State University, the M.S. degree in industrial and systems engineering from the Georgia Institute of Technology, and the Ph.D. degree in engineering science with electrical engineering focus from The University of Toledo. He is currently a Full Professor with the Department of Bioengineering, The University of Texas at Arlington. He has over 35 years of industrial and academic experience with a focus on biological signal processing and development of medical devices. He is an inventor on nine U.S. patents and a Charter Fellow of the National Academy of Inventors. He is also a Fellow of the American Institute for Medical and Biological Engineering (AIMBE) and the Institute of Electrical and Electronics Engineers (IEEE). He is a member of Tau Beta Pi (The Engineering Honor Society), Phi Kappa Phi (The Collegiate Honor Society), Sigma Xi (The Scientific Research Society), the American Society for Engineering Education (ASEE), the Biomedical Engineering Society (BMES), and the American Society of Mechanical Engineers (ASME).